AQUIFER PROJECT: “Innovative instruments for an integrated management of groundwater in a context of an increasing scarcity of hydrological resources”

Historical and recent patterns of groundwater recharge in the Campo de Cartagena Quaternary aquifer by combining hydrological modelling and satellite data

Patrones históricos y recientes de la recarga de aguas subterráneas en el acuífero cuaternario del Campo de Cartagena, mediante la combinación de modelos hidrológicos y datos satelitales

Date: 30/05/2023

This study has been carried out within the framework of the project Interreg-Sudoe AQUIFER. The partnership is composed by CUADLL (Comunitat d'usuaris d'aigua de la vall baixa i delta del Llobregat), CWP (Catalan Water Partnership), CRCC (Comunidad de Regantes del Campo de Cartagena), BRGM (Bureau de Recherches Géologiques et Minières), Aqua-Valley, ISA-LEAF (Instituto Superior de Agronomía de la Universidad de Lisboa), AR (Águas do Ribatejo), PPA (Associação Parceria Portuguesa para a Água) and CN IGME-CSIC (Instituto Geológico y Minero de España) as lead partner.

This report has been written by FutureWater as part of a consultancy contract signed with the CN IGME-CSIC in the framework of the AQUIFER project, supervised by Dr. José Luis García Aróstegui, IGME-CSIC scientific head and supported by Dra. Virginia María Robles Arenas.

This report should be cited as:

Contreras, S., García-Aróstegui, J.L., Robles-Arenas, V., Hunink, J.E., 2023. Historical and recent patterns of groundwater recharge in the Campo de Cartagena Quaternary aquifer by combining hydrological modelling and satellite data. AQUIFER Project (SOE4/P1/E1045). 61 p.

SYNTHESIS

The AQUIFER project, “Innovative instruments for the integrated management of groundwater in a context of increasing scarcity of water resources” is funded by Interreg SUDOE V (2014-2020) programme. The main objective of AQUIFER is to capitalize, test, disseminate and transfer innovative practices for the preservation, monitoring and integrated management of aquifers that are helpful when making decisions about the management of groundwater resources, improve technology transfer to local agents, create new synergies and develop common tools in a context of scarcity of water resources and environmental threats.

The Project is divided in 4 work packages. This report is the second deliverable of the activity 1.3 Analysis and collection of complementary data of pumping, evaluation of recharge with satellite and agrometeorological data. It is focused on the Campo de Cartagena-Mar Menor pilot case by improving the quantification of the recharge of the Quaternary aquifer of Campo de Cartagena using an innovative approach, which is able to combine agrometeorological and satellite-based datasets in an open-source simulation environment. Recharge estimation derived from this study are being taken as inputs into a hydrogeological model, which simulate the groundwater flow dynamics in the Quaternary aquifer. The hydrogeological model development is described in the deliverable E 2.1.1 Report and hydrogeological model of Campo de Cartagena-Mar Menor.

Table of contents

Table of figures

Tables

1 Introduction

1.1 Background

The Mar Menor, the largest coastal lagoon along the Spanish Mediterranean coast, has been affected for years by continuous inflows of water and nutrients derived from intensive agricultural, and urban and tourism development in its drainage basin known as the Campo de Cartagena. As consequence of the massive inputs of nutrients since the 1970s-80s, waters in this lagoon ecosystem reached high levels of eutrophication, and several events of algal blooms and fish kills took place since 2016 (Jiménez-Martínez et al., 2016; Sandonnini et al., 2021). Different social and policy narratives has been constructed to unravel the origin and source of the nutrient incomes and their relative contribution to the lagoon pollution (Cabello & Brugnach, 2023; Guaita-García et al., 2022). A better understanding of the historical and current drivers that control the hydrological and hydrogeological functioning of this complex socio-ecosystem is critical as a first step for identifying the most effective and sustainable management strategies.

The AQUIFER project (funded by InterregV-SUDOE Programme) aims to capitalize, test, fund and transfer innovative practices of conservation, monitoring and integrated management of aquifers to support the decision making process in groundwater resource management. With the improvement and transferability of technology to local stakeholders, the creation of synergies between social agents, and the development of common tools in a context of water scarcity and growing environmental pressures. This study focuses on the Campo de Cartagena-Mar Menor pilot case by improving the quantification of the recharge of the Quaternary aquifer of Campo de Cartagena using an innovative approach, which is able to combine agrometeorological and satellite-based datasets in an open-source simulation environment. Estimates of recharge derived from this study are being taken as inputs into a hydrogeological model which simulate the groundwater flow dynamics in the Quaternary aquifer (out of the scope of this analysis).

In recent years, several studies have quantified the main hydrological components of the Campo de Cartagena catchment, including the estimation of spatially-distributed recharge figures to the Quaternary aquifer, and the groundwater discharge to the Mar Menor lagoon. Figures of the main components of the surface water balance and estimates of recharge or

deep percolation are collected in Table 1. In general, very different values for recharge and groundwater discharge have been derived from these studies. These large discrepancies may be partially explained by usage of different conceptual modelling frameworks, but also by the general lack of reliable observations (streamflow or water level in wells) available for calibration and validation purposes.

1.2 Objective of this report

This report aims three specific objectives:

(1) To review a set of hydrological simulation tools as potential candidates for the purposes of this study. The final selection of a modelling tool rests on a SWOT analysis that analyses the pros and cons of each candidate for the local context.

(2) To improve and update the quantification of the main water balance components at the basin scale in recent times (2000-2010 period), including the daily and spatially distributed quantification of vertical (actual evapotranspiration, and root percolation) and lateral fluxes (surface runoff and root throughflow). The simulation exercise performed in this study uses the most recent version of the SPHY model, fully adapted to the local conditions, and focuses only on the soil-root zone domain. The water that drains from the bottom of the root zone towards deep soil layers, or root percolation in the SPHY code, is taken here as the potential groundwater recharge (or recharge in transit) to term. Therefore, in this study, the terms root percolation, potential groundwater recharge, or simply groundwater recharge are used interchangeably. A calibration, sensitivity and verification process with independent observations is provided at this stage.

(3) To simulate the hydrological behaviour of the basin for the historical period 1951-1999. Once calibrated, the model is forced with inputs parameters that illustrate the impact of different drivers of change accounted in the basin since 1950s. It is hypothesized that different patterns of recharge are expected at different subperiods identified by the onset of water from the Tajo-Segura interbasin aqueduct, and the implementation of farming practices addressed to reduce irritation water losses and crop water consumption. These subperiods (Table 2) have been established to cope with the most influential drivers of change identified in the region (Jiménez-Martínez et al., 2016; MITECO, 2019)

Table 1. Review of main hydrological components of the water balance for the Campo de Cartagena catchment according to the most recent studies conducted in the region. All variables in mm/year.

All in mm/year	IGME (1991)	Contreras et al. (2017)	Domingo-Pinillos et al. (2018)	Puertes et al. (2021)	Senent-Aparicio et al. (2021)
Model		**SPHY-CC (v0)**	**Visual-MODFLOW**	**TETIS**	**SWAT**
Period of reference	1940 – 1989	2001 - 2016	2000-2018	2003 - 2016	2003 - 2019
Area (km2)	1,135	1,120	1,135	100	~1,000
Precipitation		279	310	281	293
Interception		5			
Surface runoff		5		33	35
Irrigation		91		179	185
Actual evapotranspiration		286		**393**	411
Percolation	**61**	**71**	***89***	**34**	**27**
as Rainfall recharge	*41*		*35*		
as Irrigation return flows	*20*		*54*		

Table 2. Period of interest for simulating changes in potential recharge in the Campo de Cartagena catchment.

Simulation period	Remarks
1951–1979	Dominance of dryland farming. Small irrigation development that relies on groundwater abstraction with traditional infrastructure (molinos). Low efficiencies in irrigation (mainly flood irrigation)
1980–1999	Rapid irrigation development due to the onset of Tajo-Segura waters. Moderate irrigation efficiencies with increasing dominance of drip irrigation over flood irrigation
2000–2020	Highest irrigation efficiencies at the farm level, and other irrigation practices to reduce crop water consumption.

2 Methodology

2.1 Model selection

Firstly, a review and SWOT analysis has been performed to identify the most suitable modelling tool for the quantifying the water balance in the region of interest.

The number of existing hydrological models is probably in the tens of thousands (Droogers and Bouma 2014). This high diversity has been seen as the “plethora of hydrological models” (Clark et al., 2011). Several reviews covering this diversity can be found in technical and scientific literature (Addor & Melsen, 2019; Horton et al., 2022). As a common thumb rule, the selection of a model should be driven by two criteria: its parsimony (the model should not be more complex than necessary), and its adequacy to serve to the problem at hand (should be fit-for-purpose) (K. Beven & Young, 2013).

For this study, a small suite of hydrological models (SPHY, TETIS, GIS-BALAN, SWAT) have been pre-selected and evaluated as potential candidates. All these models, except the GIS-BALAN code, have been previously applied in the region of interest in the frame of different studies (see section 1.2). Table 1 collects an overview of the most relevant features and capabilities of each model including (1) the number and detail of the processes simulated, (2) the scale and resolution of application, and (3) the way they are implemented. Main features and characteristics of each model are described in the following subsections.

Table 3. Pros (+) and cons (-) of selected hydrological models. The score system evaluates each model according to (i) processes that are integrated, (iii) scale of application, and (iv) implementation.

	SPHY (v2.0)	SPHY-CC	TETIS	GIS-BALAN	SWAT
Processes					
Rainfall-Interception-Runoff	+	+	+	+	+
Evapotranspiration	+	+	+	+	+
Dynamic vegetation	+	+	+	-	
Irrigation[a]	-	+		-	
Unsaturated flow					
Groundwater flow	+	-	+	+	
Snow	+	-			+
Routing	+	-	+		+
Sediment submodel	+	-	+	-	+
Nitrogen cycle submodel	-	-	+	-	+
Water allocation (dynamic modelling)	-	-	-	-	+
Scale of application					
Spatial structure [b]	FD	FD	FD	SD	SD
Subunit parameterization	+	+	+	-	+
Time resolution [c]	dd	dd	dd	dd	dd & ev
Automatic calibration	-	-	+	+	+
Implementation					
Open source	+	+	-	-	+
Remote sensing inputs	+	+	-	-	
GIS-based	+	+	-	+	+
Local implementation (Campo Cartagena) [d]	+	+ (p)	+ (p)	-	+
Public documentation	+	-			
User community / Scientific recognition [e]	151	-	327	85	>5000

[a] It refers to the inclusion of an automatic routine able to simulate the irrigation inputs in croplands to meet the vegetation water requirements.

[b] Spatial structure: FD = conceptual - fully-distributed; SD: physically-based semi-distributed

[c] Time resolution: dd = daily; ev = event-based

[d] (p) = partially (e.g. surface catchments, subcatchment)

[d] Number of references found in Google Scholar using the name of the model and "hydrological model" (e.g. *"SPHY" AND "hydrological model"*).

2.1.1 Models included in the review

2.1.1.1 SPHY

2.1.1.1.1 Description

SPHY is an open-source, spatially-distributed, bucket-type model in which the main terrestrial hydrological processes are conceptually quantified by simulating the changes in water storages and fluxes over time and space (Terink et al., 2015). SPHY is written in python programming language using the open-source PCRaster dynamic modeling framework[1] (Karssenberg et al., 2001). SPHY integrates under the same modelling framework most of the key components existing in other well-tested models as SWAT (Gassman et al., 2007), PCR-GLOBWB (Van Beek et al., 2011), SWAP (Dam et al., 1997) and HimSim (Immerzeel et al., 2012). Recently a new a soil erosion routine based on the process-based Morgan-Morgan-Finney erosion model (Morgan & Duzant, 2008) has been fully integrated in SPHY that allows evaluating the impacts of land use, land management and climate conditions on erosion and sediment yield from local to regional scales (Eekhout et al., 2018). The current version available in Github is v3.0 (https://github.com/FutureWater/SPHY).

SPHY is grid based and cell values represent averages over a cell. Subgrid variability is allowed to take into account the presence of glacier, snow or land surface. Land surface can consist of vegetation, bare soil, or open water. The dynamic vegetation module accounts for a time-varying fractional vegetation coverage, which affects processes such as interception, effective precipitation, and potential evapotranspiration.

The soil is simulated adopting a bucket structure similar to VIC model (Liang et al., 1996). It consists of an upper soil storage (root zone), and intermediate storage (vadose zone), and a groundwater storage (saturated zone). In SPHY, precipitation at each grid-cell can be simulated in the form of rain or snow, depending on the air temperature. Precipitation that falls on land surfaces can be intercepted by vegetation (canopy interception) and evaporated in part or whole. The snow storage is updated with snow accumulation and/or snowmelt. A part of the liquid precipitation is transformed into surface runoff, whereas the remainder infiltrates into the soil. The resulting soil moisture is subject to evapotranspiration, depending on the soil properties and fractional vegetation cover, while the remainder contributes to river discharge

[1] https://pcraster.geo.uu.nl/

by means of lateral flow (interflow) from the root and vadose buckets, and baseflow from the groundwater layer. The cell-specific runoff, which becomes available for routing, is the sum of surface runoff, lateral flow, baseflow, snowmelt and glacier melt. All the processes represented in SPHY are illustrated in Figure 1.

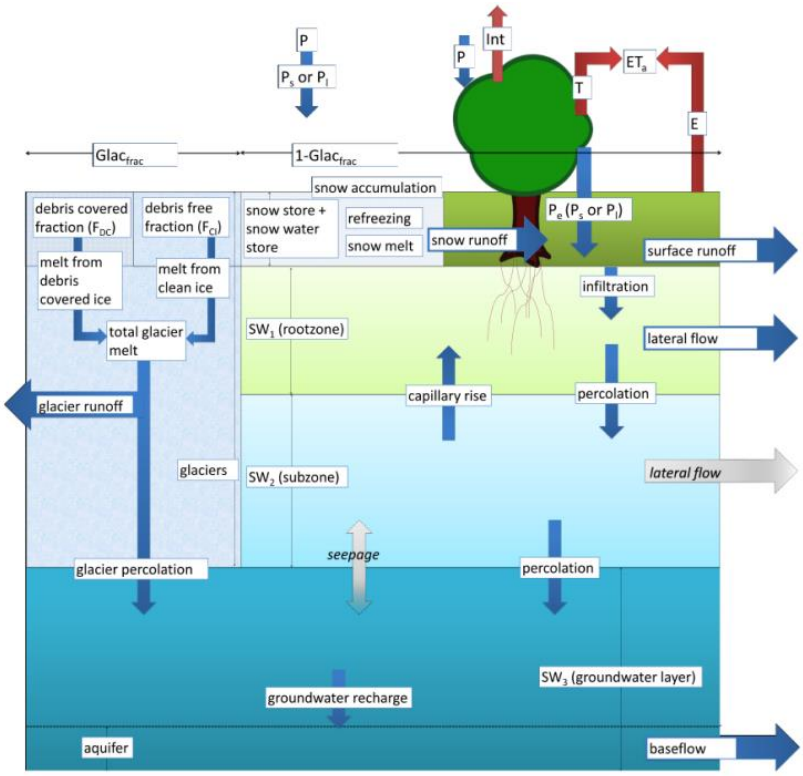

Figure 1. SPHY flowchart. Fluxes in grey are only incorporated when the groundwater module is not used.

Two flow routines are possible in SPHY depending of the presence of lakes or reservoirs. If no lakes are present, then the user can choose a simple flow accumulation routing scheme: for each cell, the accumulated amount of water that flows out of the cell into its neighboring downstream cell is calculated. This accumulated amount is the amount of water in the cell itself plus the amount of water in upstream cells of the cell and is calculated using the flow direction network. If lakes are present, then the fractional accumulation flux routing scheme is used; 12 depending on the actual lake storage, a fraction of that storage becomes available for routing and is extracted from the lake, while the remaining part becomes the updated actual lake storage. The flux available for routing is routed in the same way as in the simple flow accumulation routing scheme.

A simplified and local-tailored version of the SPHY code was applied in the Campo de Cartagena catchment in the framework of former projects (SIRRIMED, link) and consultancy activities (technical assistance to Arco Sur-Mar Menor Irrigation Community, link). In the SIRRIMED project, the major aim was to evaluate the overall water balance at the catchment scale, while in the Arco-Sur was to quantify the spatial distribution of the potential recharge to the Quaternary aquifer and its coupling with a hydrogeological model. Results from these studies were published in technical reports (Contreras et al., 2014, 2017) and scientific journals (Alcolea et al., 2019; Jiménez-Martínez et al., 2016). During these commitments, a novel irrigation module was developed able to quantify irrigation water supplies based on remote sensing analysis and soil moisture dynamics.

2.1.1.1.2 Strengths

- Open source and software code in public domain (Github)
- Good representation of most hydrological processes
- High flexibility and wide range of applicability
- Able to ingest remote sensing datasets and variables (e.g. NDVI)
- GIS pre-processor (QGIS plugin)
- User manual and technical manuals are available

2.1.1.1.3 Limitations

- Lack of irrigation routine in SPHY (v2.0) (this routine is only available for particular applications in the region but has not been fully integrated in the main code).
- High number of parameters

2.1.1.2 TETIS

2.1.1.2.1 Description

TETIS is a hydrological-sediment spatially-distributed conceptual model (Francés et al., 2007) able to simulate hydrological processes at sub-daily (floods and erosion) and daily (water resources assessment) timescales.

The hydrological routine of TETIS is based on a 5-level tank structure, in which each spatial unit or cell is interconnected vertically and horizontally, representing hillside and aquifer processes respectively. the Most relevant hydrological processes, including canopy interception, snow melting, evapotranspiration, infiltration, direct runoff, percolation, interflow, base flow and deep underground flow (Figure 2). The aquifer process is represented by a single tank.

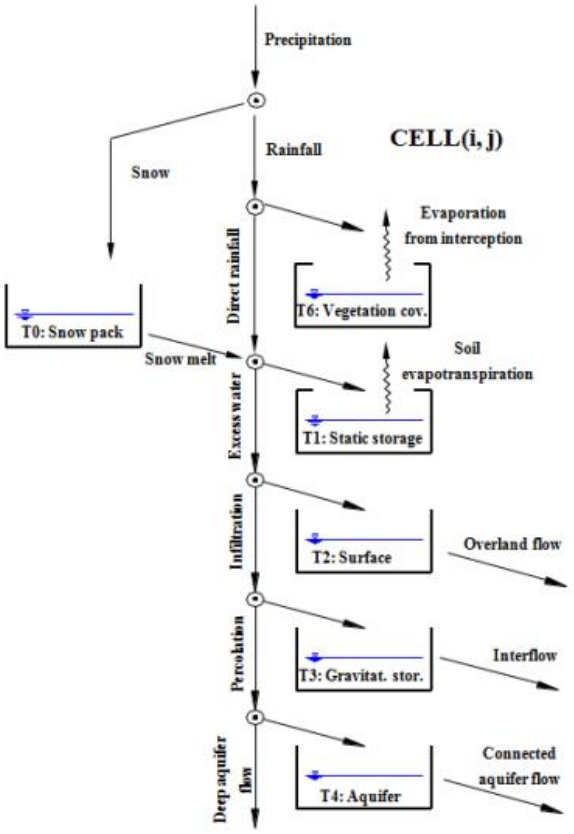

Figure 2. Conceptual scheme of TETIS model at cell.

Tank 0 (T0) represents the canopy interception process (only evaporation), while T1 refers to soil static storage (i.e., below field capacity), in which evapotranspiration is the only output flux. Water moves downwardly as long as the tank vertical outflow capacity is not exceeded. T2 is superficial water storage from which surface runoff is generated, while T3 is gravitational storage (i.e., above field capacity) from which the interflow is generated. Both, surface runoff and interflow fluxes represent the surface runoff process of TETIS. Finally, T4 represents the

aquifer. T2, T3 and T4 act as simple linear reservoirs and their outflows are routed to the corresponding tank of the downstream cell. T5 represents the river netflow.

Direct surface runoff (or overland flow), interflow and baseflow are connected to the river network by defining two threshold areas: the hillslope and the river network. Additionally, the river network is subdivided into gullies and channels. Hillslope fluxes (overland flow and interflow) are routed to the T2 and T3 tanks of the downstream cell, unless they reach a gully cell, in which case, flows are routed to the river channel tank, T5. Likewise, the base flow is routed to the T4 tank of the downstream cell, until it reaches a river channel cell, in which case, it is also routed to T5. The flux propagation in the fluvial network is solved by the Geomorphological Kinematic Wave.

TETIS rests on dynamic and static input data, all in raster format. Dynamic layers consist of temporal series of precipitation, potential evapotranspiration and temperature (the latter for the sub-model of snow melting). Static layers consist of a digital elevation model and maps with the characteristics of the rooted-soil and subsoil zones. The latter is obtained from soil studies, vegetation cover, geological maps, soil datasets and reports, hydrogeological maps and additional auxiliary data which may be relevant for the region.

Irrigation is included in TETIS through three methods or typologies: drip, sprinkler and flood irrigation. Drip and flood irrigation are directly added to the direct rainfall flux (not any fraction is lost due to direct evaporation after canopy interception), while sprinkler irrigation is added to the precipitation flux (it can be evaporated from the canopy storage and from the soil zone).

The TETIS model presents a split structure for its effective parameters, in which the effective value in a cell of a parameter is the result of the multiplication of the value of the corresponding map by a correction factor, which is common for all cells and different for each parameter. Therefore, the number of variables to be calibrated is reduced to 9 (eight hillside and aquifer processes, and one for the flux routing along the river network). These correction factors are the values that must be found through automatic calibration.

Additionally, TETIS has a powerful automatic calibration algorithm for its input parameters and initial stage conditions which greatly facilitates its practical implementation. For the introduction of the information and visualization of results, it has an interface developed in the Visual Studio environment.

More info about TETIS can be found at link

2.1.1.3 GIS-BALAN

GIS-BALAN (Samper et al., 2007) is a semi-distributed hydrological code specifically designed for the evaluation of water resources. It simulates the daily hydrological processes in the soil, in the unsaturated zone, and in the aquifer, evaluating sequentially the components of the water balance (Figure 3). The VISUAL-BALAN allows to discretize the basin into homogeneous zones in which physical, climatological and land use are considered uniform. For each zone, balances are calculated independently in the root-soil zone, the unsaturated zone, and the aquifer, assuming that there is no interaction between the zones. The consideration of homogeneous zones allows to take into account the spatial variations of the parameters and of the climatology within the basin.

Canopy interception is computed from precipitation. The net precipitation, once the interception is discounted), the irrigation water inputs and the snowmelt water are the main water inflows to the upper soil layer. Infiltration can be calculated using the Horton method or the SCS Curve Number. Surface runoff is computed as the residual between the total water available for infiltration and the actual infiltration. Water infiltrated increases the soil moisture content from which evapotranspiration (ETR) and the recharge in transit (or percolation) is computed. Percolation reaches the vadose zone.

In GIS-BALAN potential evapotranspiration values can be directly entered by user, or computed according to different climate-driven methods (Thornwaite, Blanney-Criddle, Makkink, Penman, Turk, and Hargreaves). Actual evapotranspiration is computed from potential evapotranspiration values using the original Penman-Grindley method or several slightly modified variants.

GIS-BALAN integrates two mechanisms of water percolation generation: a) a preferential-flow component, which simulates the infiltration of water through the root soil zone through cracks and/or macropores; and b) a diffuse-flow component, which simulate a Darcian flow according to the Darcy's law and which depends on the field capacity and hydraulic conductivity of soil.

GIS-BALAN incorporates a conceptual model of flow in the unsaturated zone through which water can flow horizontally (interflow) and evaporated downward, or moves vertically up to reach the aquifer or saturated zone (recharge). For the calculation of recharge, a formulation of Darcy's Law is taking into account (it assumes that the unsaturated zone behaves as a “virtual” hanging aquifer).

Finally, GIS-BALAN simulates the saturated zone as an unicellular aquifer or a multicellular-connected aquifer. The flow between cells is calculated using an explicit finite difference scheme that approximates the solution of the 1-D flow transient equation. The baseflow is the total flux that drains from the aquifer to the riverbed or to another water body (lake, wetland). Changes in water storages in the aquifer (in depth units) is related to the change in the piezometric level Δh through the equation ΔVa = S Δh, being S the aquifer storage coefficient.

The total output flux of the basin is computed as the sum of the surface runoff, interflow and baseflow. GIS-BALAN incorporates an automatic procedure of parameter calibration by minimizing an objective function (least squares) that rests on the Powell's multidimensional algorithms. Sensitivity analyses are also allowed.

Figure 3. Conceptual scheme of the GIS-BALAN model.

More info about GIS-BALAN and former developments at https://ofertatec.udc.es/directorio/empresa/gis-balan-v1-0

2.1.1.3.1 Strenghts

- Groundwater oriented-calibration (using groundwater levels)

2.1.1.3.2 Limitations

- Lack of vegetation dynamic module
- Unability to include remote sensing data (NDVI)
- Commercial license (no open-source)

2.1.1.4 SWAT

SWAT is a basin-scale, physically-based and continuous-time model that operates on a daily time step and is designed to predict the impact of management on water, sediment, and agricultural chemical yields in ungauged watersheds. Major model components include weather, hydrology, soil temperature and properties, plant growth, nutrients, pesticides, bacteria and pathogens, and land management (Gassman et al., 2007). In SWAT, a watershed is divided into multiple subwatersheds, which are then further subdivided into hydrologic response units (HRUs) that consist of homogeneous land use, management, and soil characteristics. The HRUs represent percentages of the subwatershed area and are not identified spatially within a SWAT simulation. Alternatively, a watershed can be subdivided into only subwatersheds that are characterized by dominant land use, soil type, and management

Climatic inputs used in SWAT include daily precipitation, maximum and minimum temperature, solar radiation data, relative humidity, and wind speed data, which can be input from measured records and/or generated. Relative humidity is required if the Penman-Monteith or Priestly-Taylor ET-routines are used; wind speed is only necessary if the Penman-Monteith method is used. Measured or generated sub-daily precipitation inputs are required if the Green-Ampt infiltration method is selected. The average air temperature is used to determine if precipitation should be simulated as snowfall. The maximum and minimum temperature inputs are used in the calculation of daily soil and water temperatures.

In SWAT, the overall hydrologic balance is simulated for each HRU, including canopy interception of precipitation, partitioning of precipitation, snowmelt water, and irrigation water between surface runoff and infiltration, redistribution of water within the soil profile, evapotranspiration, lateral subsurface flow from the soil profile, and return flow from shallow aquifers. Estimation of areal snow coverage, snowpack temperature, and snowmelt water is based on the approach described by Fontaine et al. (2002).

SWAT estimates surface runoff from each HRU as the combination of daily or event (hourly) rainfall and by using the curve number (CN) or the Green-Ampt (GA) method. Canopy interception is implicit in the CN method, but it is simulated when GA method is selected.

A storage routing technique is used to calculate redistribution of water between layers in the soil profile. A bypass flow can be simulated for soils characterized by cracking. Perched water tables in HRUs that have seasonal high water tables can be also simulated. Potential ET can be estimated using the Penman-Monteith, the Priestly-Taylor, or the Hargreaves method. Alternatively, external ET values can be also be ingested for a simulation run.

Recharge below the soil profile is partitioned between shallow and deep aquifers. Return flow to the stream system and evapotranspiration from deep-rooted plants (termed “revap”) can occur from the shallow aquifer. Water that recharges the deep aquifer is assumed lost from the system.

Simulation of irrigation water on cropland can be simulated on the basis of five alternative sources: stream reach, reservoir, shallow aquifer, deep aquifer, or a water body source external to the watershed. The irrigation applications can be simulated for specific dates or with an auto-irrigation routine, which triggers irrigation events according to a water stress threshold.

Flows are summed from all HRUs to the subwatershed level, and then routed through the stream system using either the variable-rate storage method or the Muskingum method, which are both variations of the kinematic wave approach.

More info about SWAT can be found at https://swat.tamu.edu/

2.1.1.4.1 Strenghts

- Source and Software code in public domain
- Simulates agricultural practices, pollutant loading, downstream impacts, an
- GIS-based APIs for MapWindows and QGIS
- Extensively used around the world (>700 peer review articles)
- Calibration, uncertainty and sensitivity analysis available through a separate program (SWAT CUP)
- User manual and technical manuals are available

2.1.1.4.2 Limitations

- Semi-distributed model. Spatial representation of HRUs ignores pollutant routing within a sub-watershed
- High level of empiricism (model formulas)
- Snowmelt model routine limited
- Erosion and sediment transport model routine limited
- Not applicable for 2D or 3D hydraulics applications

2.1.2 Summary and final selection

For the final selection phase several criteria were qualified, including: a) model availability, b) type of model, c) input data requirements, d) spatial and temporal distribution, e) model calibration process, f) additional features of interest, or g) user community/assistance available.

Table 3 collects the most relevant requirements that are necessary to meet with the needs identified in this study. According to the number of requirements fulfilled, the SPHY model was the code finally adopted for addressing the analysis. However, the selection of the SPHY code (v3.0) would require: 1) the integration of the irrigation routine developed in previous studies, and 2) some additional adjustments and developments for getting the highest level of model parsimony for this analysis.

Table 3. Main model requirements for Campo de Cartagena study.

Technical requirement	SPHY	TETIS	GIS-BALAN	SWAT
Vegetation Dynamic modelling	Y	Y	N	N
Irrigation submodule (inference)	Y	Y	N	N
Remote sensing inputs	Y	N	N	N
Sediment simulation	Y	Y	N	Y
Open-source and public code	Y	N	N	Y
Documentation and training	Y	Y	Y	Y
Calibration with groundwater observations	N	N	Y	Y
TOTAL	6 / 7	4 / 7	2 / 7	4 / 7

2.2 Model description

A brief description of SPHY was provided in section 2.1.1.1, while in this section more emphasis is given to the details on how the water balance and main hydrological components are computed.

2.2.1 Water Balance and soil moisture dynamics

The soil water dynamics in SPHY is simulated for a vertical profile which is divided into three layers: the shallow soil zone, the deep soil layer, and the groundwater zone. The two uppermost layers simulates the fluxes in the soil vadose zone. In this study, only processes in the shallow soil zone are taken into account. The water balance of the first soil layer is computed as:

$$Root\_S_t = Root\_S_{t-1} + Pre_t + Irr_t - Eta_t - SRof_t - RTfw_t - RPer_t + CapR_t$$

Equation 1

In Equation 1, $Root\_S_t$ and $Root\_S_{t-1}$ are the soil moisture contents in the root zone in day t and t-1, respectively. Pre_t is the precipitation on day t, Eta_t is the actual evapotranspiration, $SRof_t$ the surface runoff, $RTfw_t$ is the root throughflow (or lateral flow or interflow from the root zone), $RPer_t$ is the root percolation, or potential recharge, and $CapR_t$ is the capillary rise from the deep unsaturated zone. All components are computed on a daily basis and in mm.

Water dynamics, redistribution and storage in soils depend on the soil pore space and pore-size distribution, which is mainly driven by soil texture and structure. Three soil moisture states, *saturation*, *field capacity* and *permanent wilting point* are used to describe the soil water status in SPHY (O'Green, 2013). Saturation (*Sat*) refers to the point over which water movement is mostly controlled by gravitational forces. Water flows through the soil macropores and downward along the soil profile or laterally downslope. Field capacity (*Fc*) represents the soil water content retained against the force of gravity by matric forces (in micropores and mesopores) at tension of -0.033 Mpa. Water held between saturation is usually subject to free drainage over short time periods and it is generally considered unavailable to plants. This free water is termed drainable porosity. In contrast, much of the water held at field capacity is available for plant uptake and use through evapotranspiration.

The permanent Wilting Point (*Wp*) represent the status in matric forces hold water too tightly for plant extraction (-1.5 Mpa). Water held between *Fc* and *Wp* is retained against the force of gravity, but not so tightly to impede its abstraction by plants. However, water held at potentials below PWP (< -1.5 Mpa) are not available for use by most plants. An intermediate soil moisture condition between the *Fc* and *Wp*, called the *Dry* point, determines the soil moisture threshold below which plant starts to be stressed and evapotranspiration is reduced by a stress depletion factor. From *Dry* to *Fc*, evapotranspiration is taken at its maximum rate driven by the potential evapotranspiration.

In the following sections, the different processes which control the water balance in the root zone are described.

2.2.2 Canopy Interception

Canopy interception refers to the total of water that may remain in the canopy after a rainfall event. Interception depends on the storage capacity of the canopy and the water content already stored in the canopy from the previous day. Canopy interception is computed as:

$$Cano\_S_t = \min(Cano\_S_{max}, Cano\_S_{t-1} + Pre_t)$$

Equation 2

being $CanoS_t$ (mm) and $CanoS_{t-1}$ (mm) the canopy water storage on days t and t-1, Pt (mm) the amount of precipitation on day t, CanoSmax is the maximum water storage capacity that vegetation can stored. In case that the capacity of the canopy is exceeded by the onset of a rainfall, the water that drains to the soil is known as effective precipitation.

$$PreE_t = \max(0, Cano\_S_{t-1} + Pre_t - Cano\_S_{max})$$

Equation 3

The remaining amount of water that is not effective precipitation, is already available for interception. Interception loss will depend on the atmospheric demand for open water evaporation. A commonly used value for the atmospheric demand for open water evaporation is 1.5 (Allen et al., 1998) which is derived from the ratio between 1 and the mean pan evaporation coefficient Kp (~0.65). Interception can now be calculated using:

$$Int_t = \min(1.5 * Etr, Cano\_S_t)$$

Equation 4

being Int_t (mm) the canopy interception on day t, and Etr (mm) the reference evapotranspiration on day t. After subtracting the water losses due to interception, the actual water content in the canopy is updated.

The establishment of the maximum canopy storage capacity ($CanoS_{max}$) referred in Equation 3 is based on LAI (Leaf Area Index)

$$Cano\_S_{max} = 0.935 + 0.498 * LAI - 0.00575 * LAI^2$$

Equation 5

being,

$$\mathrm{LAI} = \mathrm{LAI}_{\max} \cdot \frac{\log(1 - \mathrm{FPAR})}{\log(1 - \mathrm{FPAR}_{\max})}$$

Equation 6

being LAI_{max} the maximum LAI expected for a particular vegetation type (values are similar to the ones shown in Table 4), and FPAR is the Fraction of absorbed Photosynthetically Active Radiation which is computed using a time-variable NDVI-based function as

$$FPAR = min\left(\frac{(SR - SR_{min})(FPAR_{max} - FPAR_{min})}{(SR_{max} - SR_{min})} + FPAR_{min}, 0.95\right)$$

Equation 7

being

$$\mathrm{SR} = \frac{1 + \mathrm{NDVI}}{1 - \mathrm{NDVI}}$$

Equation 8

$FPAR_{max}$ and $FPAR_{min}$ adopt values of 0.95 and 0.001, respectively. FPAR and LAI are closely related: in literature, FPAR values of around 0.95 have been reported to the maximum LAI

values expected for a particular vegetation type, while FPAR close to 0 refers to a vegetation with a minimum LAI. In order to calculate FPAR, an NDVI time series is required.

Table 4. LAI_{max} values for different vegetation types (Sellers et al., 1996).

Vegetation type	LAI_{max} [-]
Needleleaf evergreen trees	8
High latitude deciduous trees	8
Mixed trees	7.5
Broadleaf evergreen trees	7
Broadleaf deciduous trees	7
Crops	6
Grass with 10 - 40% woody cover	5
Grass with <10% woody cover	5
Shrubs and bare soil	5
Moss and lichens	5

2.2.3 Surface Runoff

SPHY accounts for two mechanisms of surface runoff generation: a saturation excess-driven runoff or Hewlettian runoff (Hewlett, 1961), and an infiltration excess-driven runoff or Hortonian runoff (Horton, 1933). User is allowed to set up one of these mechanisms.

The saturation excess runoff happens when the shallow soil layer (root zone) gets saturated. This condition is met when the soil moisture exceeds the saturation point.

$$\mathrm{SRof} = Rof \begin{cases} Root\_S - Root\_S_{sat} & \text{if} \quad Root\_S > \mathrm{Root\_S_{sat}} \\ 0 & \text{if} \quad Root\_S \leq \mathrm{Root\_S_{sat}} \end{cases}$$

Equation 9

being SRof (mm) the daily surface runoff, Root_S (mm) the water content in the uppermost soil layer, and $Root\_S_{sat}$ (mm) is the total water that the topsoil can store under saturated conditions.

Infiltration-excess runoff is commonly understood as a sub-daily process that happens when the precipitation intensity exceeds the infiltration capacity of the topsoil layer. To cope with the daily simulation timescale, SPHY adopts a modified infiltration excess surface runoff equation based on the Green-Ampt formula (Heber Green & Ampt, 1911). In this formula a constant infiltration rate f (mm hr^{-1}) is firstly computed at the daily and pixel level by:

$$f = \frac{K_{\text{eff}}}{24}\left[1 + \frac{Root\_S_{sat} - Root\_S}{Root\_S_{sat}}\right]^{\lambda}$$

Equation 10

being K_{eff} the effective hydraulic conductivity (mm day^{-1}), Root_S (mm) the water content in the first topsoil layer, Root_S_{sat} the saturated water content of the topsoil, and λ is a nondimensional calibration parameter. Bouwer (1969) suggested an approximation of $K_{\text{eff}} \approx 0.5K_{\text{sat}}$.

Infiltration-excess runoff happens when the precipitation intensity exceeds the infiltration rate f (K. J. Beven, 2012). It is assumed that the highest precipitation intensity is reached in the first hour of the rain event and decreases linearly until the end of the storm. Furthermore, it assumed that precipitation intensity p(t) follows a triangular-shaped function according to:

$$p(t) = \frac{1}{2}\alpha^2 Pt + \alpha P$$

Equation 11

where α is the fraction of daily rainfall that occurs in the hour with the highest intensity, P is the daily rainfall (mm), and t is an hourly time step (hr). Total infiltration-excess runoff is finally computed as:

$$Q_{\text{surf}} = \begin{cases} \frac{(\alpha P - f)^2}{\alpha^2 P} & \text{if } \alpha P > f \\ 0 & \text{if } \alpha P \leq f \end{cases}$$

Equation 12

When the hourly precipitation intensity αP is higher than the infiltration rate f, surface runoff equals the triangular shaped area of the precipitation above the infiltration rate. The amount

of precipitation below the infiltration rate will infiltrate into the rootzone and may generate saturation-excess runoff if the saturation storage threshold is overpassed.

2.2.4 Root throughflow

This term is also known as root interflow or subsurface lateral flow. Its relevance in the water balance equation increases as higher is the slope of the land or the soil hydraulic conductivity (K. Beven, 1982). In SPHY, this hydrological component happens when there is drainable water in any of the vadose soil layers., condition that is reached when the water stored in the topsoil layer or deep vadose soil layer rootzone is higher than water storage at field capacity. The root throughflow in the root zone layer is computed as:

$$RTfw_t = \left[\left(\frac{Root\_S_t - Root\_S_{fc}}{Root\_S_{sat} - Root\_S_{fc}}\right) * v + RTfw_{t-1}\right] * \left(1 - e^{-1/TT}\right)$$

Equation 13

being $Root\_S_t$ (mm) is actual water stored in the soil layer at timestep *t*, $Root\_S_{sat}$ (mm). $Root\_S_{fc}$ (mm) is the water storage at saturation and field capacity, ϑ is the flow velocity at the outlet (mm d^{-1}) (Equation 15), $RTfw_{t-1}$ is the root throughflow in time *t-1*, and TT is the throughflow travel time which relies on the soil saturation point, the field capacity and the saturated conductivity ($Root\_K_{sat}$), as:

$$TT = \frac{Root\_S_{sat} - Root\_S_{fc}}{Root\_K_{\mathrm{sat}}}$$

Equation 14

A longer lateral flow travel time will result in a smoother streamflow hydrograph.

Finally, the flow velocity at the outlet is computed as:

$$\boldsymbol{\vartheta = Root\_K_{\mathrm{sat}} \cdot \mathrm{slp}}$$

Equation 15

being *slp* the slope of the pixel, and $Root\_K_{sat}$ the saturated hydraulic conductivity of the root zone layer.

2.2.5 Actual Evapotranspiration

Actual evapotranspiration (Eta) is the quantity of water that is actually getting off from the surface by the processes of evaporation and transpiration. In drylands, this term represents one of the major components in the water balance. The right quantification of this term is critical to understand the remaining water fluxes. Actual evapotranspiration in SPHY is computed by adopting a FAO56 method, which rest on a satellite-based Vegetation Index, the NDVI, which is used as a surrogate of the ET/crop basal coefficient.

Following the FAO56 approach, Eta is computed as:

$$Eta = Etr * K_c * K_s$$

Equation 16

being Etr the reference evapotranspiration, Kc is crop coefficient under no stress conditions, and Ks is a scalar which accounts for the reduction in evapotranspiration due to the crop stress due to water deficit or water excess.

Kc represents the crop coefficient. Pôças et al. (2020) provide a review of methods which use satellite-based indices to predict Kc values, known as Kc-VI approaches. Kc-VI approaches aim to reflect the actual growth conditions of the crops, thus encompassing the temporal variability of the coefficients (*Kc*) and their spatial variability within and between fields and even at broader scales (e.g., irrigation districts) (Pôças et al., 2020). Several studies have shown that under conditions of crop water stress or soil water deficit, the *Kc-VI* approaches represent the effects associated to growth reduction but may fail to represent the effect of plants stomata closure on ET reduction.

SPHY incorporates a dynamic-vegetation module able to simulate Kc values from satellite data. The current parameterization assumes a linear correlation between paired values of Kc-NDVI for the minimum and maximum stages of crop development.

$$K_c = K_{c\_min} + \left(K_{c\_max} - K_{c\_min}\right) \frac{NDVI_t - NDVI_{min}}{NDVI_{max} - NDVI_{min}}$$

Equation 17

In which K_{c_min}, is the minimum crop coefficient for bare soil ($NDVI_{min}$), and K_{c_max} is the crop coefficient for peak plant growth condition having nearly full ground cover (Pôças et al., 2015).

Stress for crop evapotranspiration is mainly driven by water shortage in the root zone. SPHY adopts the FAO56 approach (Allen et al., 1998) in which rootwater uptake declines when water content in the rootzone is less than a critical value which accounts for soil hydraulic and plant-specific characteristics (Figure 4).

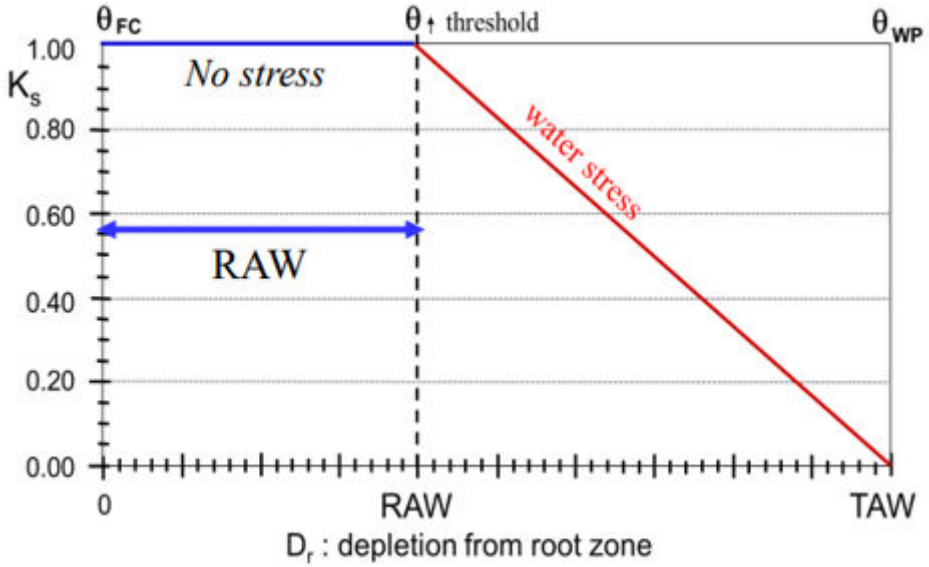

Figure 4. FAO56 Method for estimating Stress Coefficient (Ks).

Ks is computed as

$$K_s = \frac{TAW - D_r}{(1 - p_{adj}) * TAW} = \frac{TAW - D_r}{TAW - RAW}$$

Equation 18

being TAW the total available water in the rootzone (mm), Dr the root zone depletion (mm) or water shortage relative to field capacity, and p_{adj} a crop-specific adjusted depletion factor[2]

[2] Value of p is crop-specific and its final value varies according to the evaporation power of the atmosphere (Etr). For hot-dry weather conditions with high rates of Etr, p values are 10-25% less the values typically found for normal conditions. In the opposite, when Etr is low, p can be increased up to 20%. Values of p are usually tabulated for normal conditions and properly adjusted to cope with differences in drying weather conditions.

which defines the Readily Available Water (RAW) or fraction of TAW that a crop can extract from the root zone without suffering water stress.

$$TAW = S_{fc} - S_{wp}$$

Equation 19

$$D_r = S_{fc} - S$$

Equation 20

$$RAW = p_{adj} * TAW$$

Equation 21

The adjustment of the depletion factor accounts for differences in the drying power of the atmosphere (potential evapotranspiration) according to Equation 22 and it adopts values between 0.3 and 0.7.

$$p_{adj} = \max(0.3, \min(p + 0.04 * (5 - Etp), 0.7))$$

Equation 22

being *p* is the crop-specific (non-adjusted) depletion factor for normal drying conditions.

2.2.6 Irrigation

SPHY includes an irrigation module able to simulate the irrigation water applied (*Irr*) in an irrigated pixel. *Irr* values are computed based on the assumption that irrigation inputs are applied to meet the adjusted water requirements of a crop at a particular timestep. Irrigation requirements depend on soil moisture status, the irrigation strategy adopted by farmers, and the irrigation efficiency of the crop system. Irrigation efficiency factor accounts the distribution and application losses of a system.

Irrigation is computed as:

$$Irr = \frac{\mathrm{RAW} * \left(1 - MAD_f\right)}{Irr_{eff}} * Mask\_crop$$

Equation 23

$$IrrL = Irr * \left(1 - Irr_{eff}\right)$$

Equation 24

Being MAD_f a scalar which accounts the management strategy or the crop's tolerance to stress conditions. The $RAW*MAD_f$ product in Equation 23 defines the MAD (Management Allowed Depletion) term introduced by Allen et al. (1998). MAD_f values <1 are adopted when a certain tolerance to stress is allowed (e.g. crops which allow deficit irrigation), while values >1 are adopted when extra irrigation is required to avoid severe impacts due to water or salt stress conditions.

Mask_crop is binary parameter that accounts for the duration of the growing season. The parameter is set up at each simulation timestep and it adopts values of 0 (no-irrigation) or 1 (irrigation). The duration of the growing season is set up by the user according to the crop typology and the crop intensification and irrigation scheduling. The irrigation period for perennial crops/tress cover most of the year, while in row crops the length of this period relies on the cropping system (shorter in single-cropping systems than in multiple-cropping ones)

2.2.7 Runoff routing

Instead of using the St. Venant equations or the Manning equation, SPHY computes the accumulated amount of water that flows out from a pixel into its neighboring downstream cell. This approach is implemented through the *accuflux* PcRaster built-in function, which calculates for each cell the accumulated specific runoff from its upstream cells, including the specific runoff generated within the cell itself. SPHY also includes a flow recession coefficient (Kx) that aims to capture the typical delays in flows that happen due to friction or resistance forces that act along the drainage or channel network.. Using this coefficient, river flow in SPHY is calculated using the three equations shown below:

$$QTot_t^* = \frac{QTot_t \cdot 0.001 \cdot A}{24 \cdot 3600}$$

Equation 25

$$Q_{accu,t} = accuflux(F_{dir}, QTot_t^*)$$

Equation 26

$$Q_{rout,t} = (1 - kx) \cdot Q_{accu,t} + kx \cdot Q_{rout,t-1}$$

Equation 27

with $QTot_t^*$ ($m^3\ s^{-1}$) the specific runoff on day t, $Qtot_t$ (mm) is the specific runoff in water depth units on day t, A (m^2) is the the grid-cell area, $Q_{accu,t}$ ($m^3\ s^{-1}$) is the non-delayed accumulated streamflow on day t, $Q_{rout,t}$ ($m^3\ s^{-1}$) the routed streamflow on day t, $Q_{rout,t-1}$ ($m^3\ s^{-1}$) the routed streamflow on day t-1, F_{dir} the flow direction network, and kx (–) the flow recession coefficient. The kx coefficient has values ranging between 0 (fast-response catchments) and 1 (slow-response catchments). This coefficient is typically used for model calibration.

SPHY allows routing each all of those components that may contribute to the total streamflow of a basin, i.e. surface runoff, both throughflows from the root and deep soil layers, and the baseflow from the groundwater component.

2.3 Setting up – Model inputs

2.3.1 Simulation domain

The simulation domain used in this study covers the recharge area of the Quaternary aquifer of Campo de Cartagena. This area includes all the catchments that drain to the Mar Menor, including the Rambla del Albujón catchment, and the Benipila catchment in the southern side. In this study, it is assumed that the upper section of Rambla del Albujón is an isolated subcatchment hydrogeologically disconnected from the Quaternary aquifer. Hence, three large spatial domains of recharge have been defined (Figure 5): 1) Rambla del Albujón (middle and lower section) and Mar Menor catchments (yellow), 2) Rambla de Benipila catchment (green), and 3) Fuente Álamo area or upper section of the Rambla de Benipila (blue). An additional layer, composed by different "recharge" subunits have been adopted to compute the spatially-distributed figures of recharge for the hydrogeological model of Campo of Cartagena.

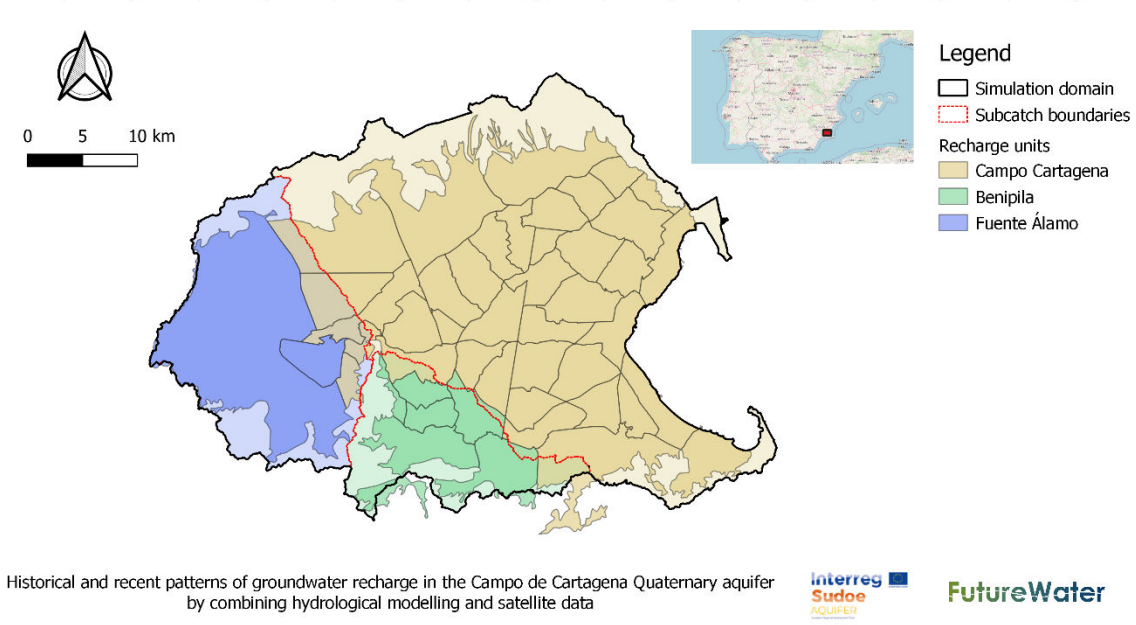

Figure 5. Simulation domain for SPHY-CC model.

2.3.2 Climate

Meteorological forcings for the SPHY-Campo de Cartagena model, hereafter referred as SPHY-CC, were retrieved from the observational climate dataset developed by the Spanish Meteorological Agency (AEMET) to support the generation of climate change scenarios[3]. The AEMET-CLIMA dataset consists of gridded data of total precipitation accumulated in 24h, and daily maximum and minimum temperatures. The native gridded dataset has a rotated projection and a spatial resolution 0.05 deg. in lat/lon (~5 km) and it covers the continental Spain for the 1951-2020 period. The dataset has been generated by using ground meteorological observations from the AEMET Climate Database and an Optimum Interpolation algorithm. Technical details are provided in Peral et al. (2017)

For the purposes of this project, raw data was collected in its native format in netCDF. A specific routine was created in SPHY to enable the automatic ingestion of netCDF files during the simulation process. The routine allows to: 1) reproject the native rotated projection of the AEMET-CLIMA dataset into a planar projection, 2) resample the native resolution of 5km into the spatial resolution of interest by applying a linear (used for precipitation) or cubic (used for

[3] https://www.aemet.es/es/serviciosclimaticos/cambio_climat/datos_diarios?w=2&w2=0

temperature) interpolation method (Table 5), and 3) generate a readable input for the PCRaster programming language.

Table 5. Overview of climatological dataset used (native and model traits).

Variable	Native dataset			Model dataset		
	Version (AEMET)	Spatial projection	Spatial resolution	Spatial projection	Spatial resolution	Resampling method
Accumulated daily precipitation	V2	Rotated pole grid	0.05 deg.	EPSG: 25830	200 m.	Linear
Minimum daily temperature	V1					Cubic
Maximum daily temperature	V1					
Average daily temperature				Computed as the mean value of Tmin and Tmax		

2.3.3 Soil

In SPHY-CC model, the soil parameters that defines the *Sat*, *Fc*, *Dry* and *Wp* conditions have been estimated using pedotransfer functions which use soil texture (relative fraction of sand, silt and clay), bulk density, and organic matter as main predictors. Maps of soil texture and bulk density were retrieved from soil type categories established for the region by Faz Cano (2003), and point texture measurements reported for the catchment in the LUCDEME project. Average values of sand, silt and clay content were adopted as representative per each soil typology. Spatial patterns of soil texture were assumed have not changed along the simulation period (1951-2020).

A map of organic matter content was retrieved adopting a LUT (lookup-table) approach based on landuse categories, and the average values of OM derived from LUCDEME's measurements.

The saturated hydraulic conductivity at the rot zone (*Root_Ksat*) was also computed using a pedotransfer function, which takes soil texture, bulk density and organic matter as main predictors.

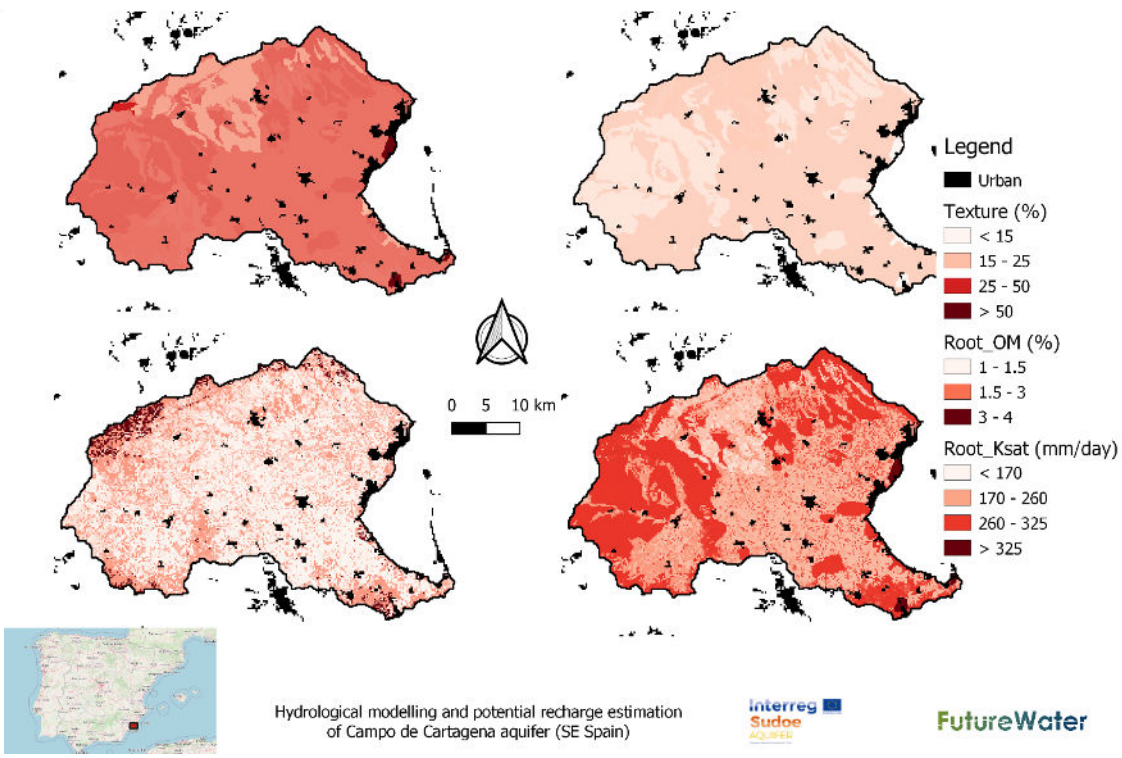

Figure 6. Root soil parameters used in SPHY-CC. Upper left: sand content (%); upper right: clay content (%); lower left: organic matter content (%); lower right: saturated hydraulic conductivity (mm/day).

2.3.4 Land Use / Land Cover

Three landuse/landcover (LULC) maps which refer to 1977, 2000 and 2020 years have been collected and prepared for the purposes of this study (Table 6). These maps have been considered as sufficient representative of the 1951-1980, 1981-2000, and 2001-2020 periods of simulation. Spatial data have been collected from three sources (Table 6):

1) For 1977, the Map of Crops and Uses at scale 1:50.000 and developed by MAGRAMA

2) For 2000, the land cover map elaborated by Carreño et al. (2015) by applying image classification on Landsat satellite imagery

3) For 2020, the LULC map derived from the SIOSE project by the Soil and Water Conservation department of the CEBAS-CSIC. 8 large LULC categories have been defined for the study region and period of analysis.

Most relevant parameters for those LULC classes are shown in Table 7.

Table 6. Sources of data employed in this study for the characterization of past and current patterns of landuse.

Landuse	Source	Representative for period
1977	MCA50[4] MAGRAMA (1977)	1951 – 1980
2000	Carreño et al. (2015)	1981 – 2000
2020	SIOSE project	2001 – 2020

Table 7. Land Use – Land Cover categories evaluated in the Campo de Cartagena basin and baseline values for SPHY input parameters.

ID	Category	LAImax	Root_depth	Crop coefficient (Kc)	ET depletion factor (p-value)	Managed Irrigation Depletion (MAD)
1	Irrigated tree crops	6	700	0.6	0.5	1.395
2	Irrigated row crops	8	300	1.0	0.3	0.53
3	Forest	8	1500	1.0	0.7	
4	Shrubland	5	500	0.75	0.6	
5	Rainfed tree crops	6	300	0.9	0.4	
6	Greenhouses	5	100	0.75	0.6	
7	Urban					
8	Water		0	1.05		

As it is shown in the Figure 7, the basin has suffered an intense change in land use:

- During the 1951 – 1979 period rainfed tree crops dominated most of the basin covering more than 80,000 ha. (63% of the total area), followed by far by shrublands (21,000 ha, 16%). Irrigated tree and horticulture crops occupied around 17,500 ha (14%). The area covered by irrigated farming started to increase abruptly after the onset of water from the Tajo-Segura interbasin aqueduct in 1980.

[4] Mapa de Cultivos y Aprovechamientos de España, escala 1:50.000. MAGRAMA (1977)

- Although with less coverage, rainfed tree crops was also the dominant LULC class in the period 1980 – 1999 (43,600 ha, 34%) followed closely by irrigated horticulture (39,500 ha, 31%) and irrigated tree crops (18,200 ha., 9%).
- In the last period from 2000 to 2020, the total area of irrigated horticulture remained very similar than in the precedent period, while the area covered by irrigated tree crops increased by 67%, up to reach more than 18,000 ha. In the simulation period, urban area increased from 5,000 ha in 1977 up to 12,600 ha in 2020.

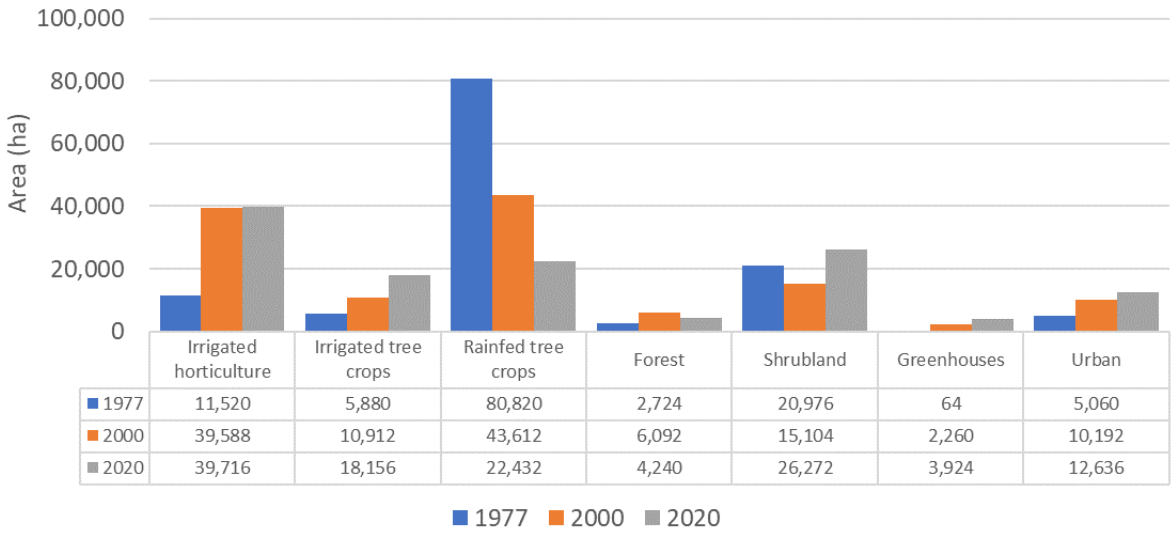

	Irrigated horticulture	Irrigated tree crops	Rainfed tree crops	Forest	Shrubland	Greenhouses	Urban
1977	11,520	5,880	80,820	2,724	20,976	64	5,060
2000	39,588	10,912	43,612	6,092	15,104	2,260	10,192
2020	39,716	18,156	22,432	4,240	26,272	3,924	12,636

Figure 7. Evolution of landuse/landcover categories in the period of interest.

2.3.5 Vegetation parameters

Vegetation dynamics plays an important role in controlling soil moisture dynamics and water balance through its influence in interception and evapotranspiration losses. In SPHY the role of vegetation is mainly approached by using the NDVI (Normalized Difference Vegetation Index), a functional indicator of vegetation greenness strongly related with the evapotranspiration term (Pettorelli et al., 2005). By inverse modelling, NDVI can be also used in irrigated lands to derive estimates of irrigation inputs. This approach has been adopted for the SPHY-CC model.

NDVI maps for the period of interest were generated using Multiple Linear Regression approach which rest on the landuse-specific relationship between observed NDVI and climate variables (precipitation and temperature) in a calibrated period. The general flowchart is shown in Figure 8. In a first stage, representative mean annual NDVI trajectories were retrieved for each landuse category found in the region at each NDVI-timestep of the year. Satellite

observations of NDVI were retrieved from the MODIS-Terra MOD13Q1 satellite product. MOD13Q1 is a product derived from the MODIS sensor onboard the Terra satellite aircraft which consists of 16-days Maximum Value Composites of NDVI. The product was collected for the 2001-2020 period. In a second stage, Multiple Linear Regression models (MLR) between the NDVI (predictand) and climate predictors (precipitation and temperature) were adjusted for each landuse category. MLR models were finally used in combination with the climate predictors and landuse/landcover for hindcasting the NDVI for all the simulation period (1951 to 2020).

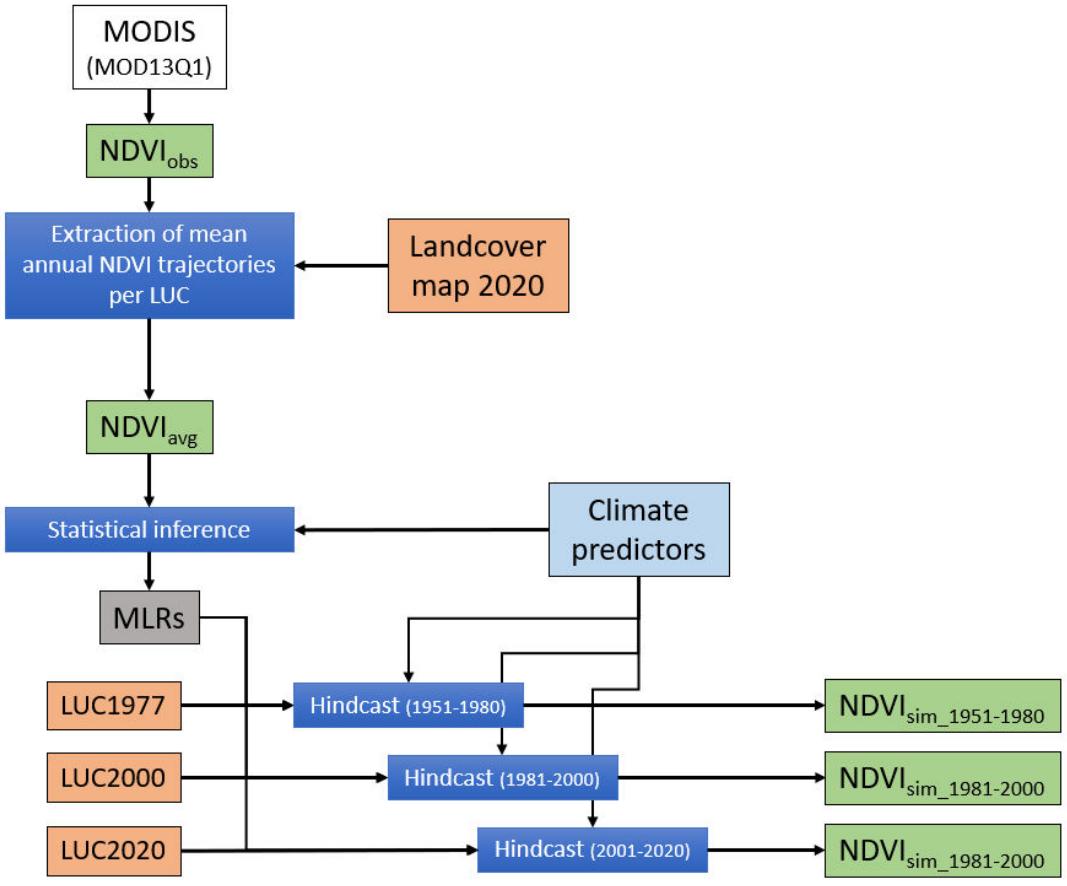

Figure 8. Flowchart for generating temporal NDVI fields.

2.3.6 Irrigation parameters

Irrigation is controlled in SPHY through Two important parameters need to be adopted in SPHY. The first accounts MAD factor which modifies the Readily Available Water used for quantifying the gross irrigation required to cope with crop water requirements and the irrigation

management strategy. The second refers to the irrigation efficiency when irrigation is applied at the farm level. Different MAD factors are adopted for irrigated croplands or land use categories, while a global irrigation efficiency is adopted for the whole system. The value of these parameters have been changed for each simulation sub-period in order to include how the irrigation system (in terms of efficiency and technology inclusion) has evolved from 1950 until current times.

2.4 Sensitivity analysis and model calibration

The sensitivity of SPHY outputs to input parameter has been evaluated. This has been addressed adopting a one-at-a-time framework, in which an input parameter is changed by a fixed scalar or selected magnitude while the others remain equal. All simulations covered the 2000-2020 period. Impact was quantified at annual scale in absolute (i.e., change in water depth units), or relative terms (i.e. change in relationship with a baseline condition).

The verification of the outputs has been addressed through an intercomparison analyses between simulated fluxes and figures collected from independent sources. Data from sources independent source consisted:

- Water balance estimates from the Contreras et al. (2017) study. Mean annual values of total evapotranspiration, irrigation inputs and total root percolation from this study were used as pseudo-observations for the validation process. Although not imperative, the search of convergence with those figures has been prioritized.

- Totals of water delivered for irrigation by CRCC[5] at sector levels. Water delivered by CRCC does not account groundwater abstractions in the region, so these figures should be taken with caution when compared with the SPHY estimates of gross irrigation.

- Streamflow measurements at 4 gauge stations located in the lower section of the Rambla del Albujón (Table 8, Figure 9). Rambla del Albujón is the axial drainage of the Campo de Cartagena. The lower sector of this water course shows a regular flow as consequence of the rise of the Quaternary aquifer water table resulting from an increase of the irrigation return flows. Additionally, close to the outlet the watercourse is also fed, through a drainage channel, with puntual inflows from a urban wastewater treatment plant. Streamflow data started to be monitored regularly since ends of 2017. During this period very few runoff events were

[5] The Irrigators Community of Campo de Cartagena.

monitored. Due to the short length of the streamflow dataset, the calibration-validation the with these observations was merely for quality control. The flow duration curves for each gauge station are shown in Figure 10.

Table 8. List of streamflow gauge stations used for the CAL/VAL process.

Station ID	Stream Name	Station Name	X_ETRS89	Y_ETRS89	Active since
06A01A1 (ID01)	Rbla Albujón	M.C. La Puebla	683796	4176860	15/02/2017
06A02A1 (ID02)	Rbla Albujón	M.C. Pzo Estrecho	678088	4177087	01/12/2016
06A03A1 (ID03)	Rbla Albujón	M.C. Rbla Albujón	671930	4176717	01/01/2017
06A04A1 (ID04)	Rbla Albujón	M.C. El Estrecho	666775	4177129	31/03/2017

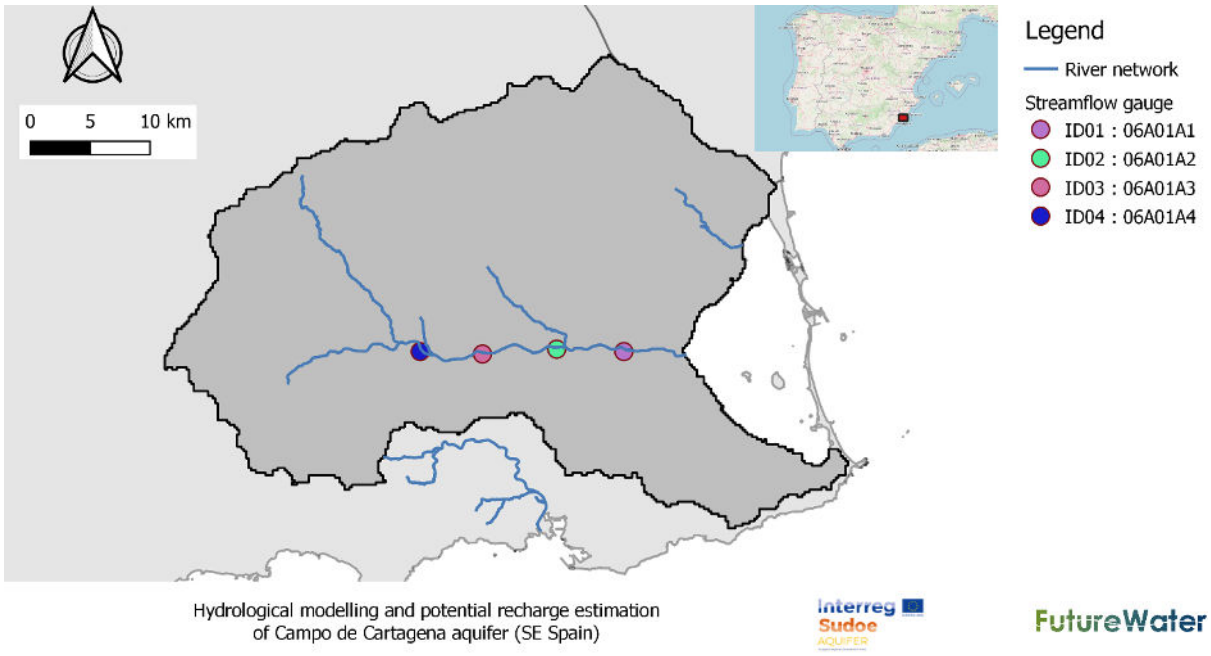

Figure 9. Location of selected streamflow gauges in Rambla del Albujón.

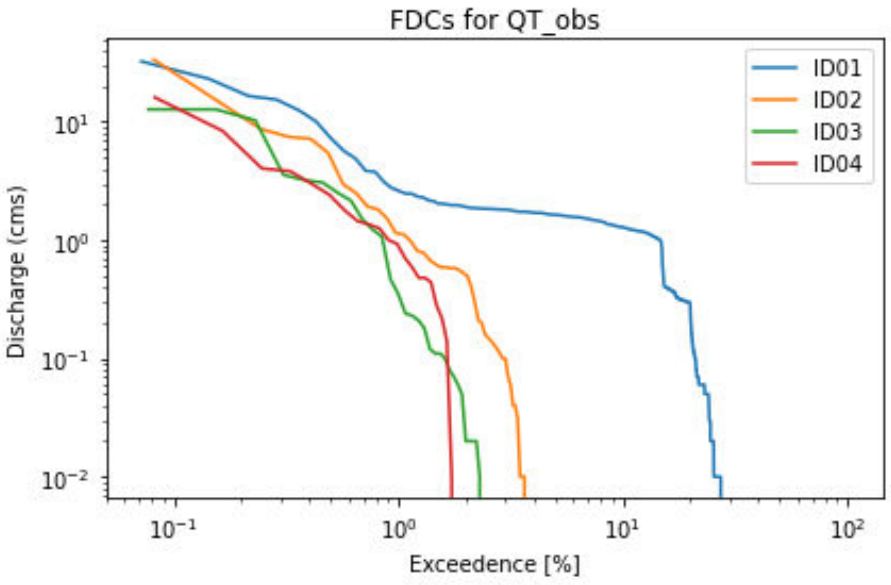

Figure 10. Flow Duration Curves for selected streamflow gauges located in Rambla del Albujón. Data extracted from the Segura River Basin Authority (SAIH platform).

The sensitivity analysis was performed to quantify the sensitive model to changes in some key SPHY parameters, and to support the calibration of the model. Based on expert-knowledge, a set of 6 key parameters were selected (Table 9). All the possible combinations were evaluated running the model at a daily timestep and for the 2000-2020 period. In total more than 2850 runs were executed with a total computing time of ~40k minutes.

2.5 Historical parameterization

For the historical simulation, several parameters were set up to evaluate the recharge dynamics due to the onset of water resources from the Tajo-Segura interbasin aqueduct, and the implementation of modern irrigation and farming practices. A brief description of these conditions is provided in Table 10.

The irrigation efficiency is a key parameter that strongly modifies the total of Irrigation Water Applied (IWA, or *Irr* in the SPHY-CC model) and return flows at the system level. High levels of irrigation efficiency (>0.90) have been reached in the Campo de Cartagena since the 2000s, being nowadays around 0.95. However, this recent fact was not the case in the past when values were around 0.6 during the 1960-70s, or 0.8 during the 1980-90s.

Table 9. SPHY parameters used in the sensitivity analysis, and the set of values finally retrieved from the Calibration/Validation procedure.

Parameter	Baseline value; Scalars of change	Water balance component	Final selection
Root_depth	[250, 400, 500, 750]	Soil moisture dynamics	500
LAImax	0,2.5, 7.5, {1:6, 2:8}, {1:2.5, 2: 3.0}	Canopy interception	{1:6, 2:8}
Root depletion fraction (p-value)	{1: 0.5, 2: 0.3}, {1: 0.3, 2:0.1}, {1: 0.7, 2: 0.5}	Evapotranspiration	{1: 0.5, 2: 0.3}
MAD	{1: 1.05, 2: 0.60}, {1: 1.25, 2: 0.80}, {1: 1.40, 2: 0.55},	Irrigation	{1: 1.25, 2: 0.8}
Irrigation Efficiency (IrrEff)	0.50, 0.85, 0.90, 0.95	Irrigation	0.90
Kx	0.15, 0.30, 0.45, 0.60	Surface runoff and root througflow routing	0.3

Table 10. Model parameter values adopted for simulating the water balance dynamics during the 1951-2020 period.

Simulation period	1951–1979	1980–1999	2000–2020
Landuse & Soil maps	1977	2000	2020
RDepth	Irrigated row crops: 0.3 m; Irrigated trees: 0.7 m		
LAImax	Irrigated row crops: 6; Irrigated trees: 8		
PFactor	Irrigated row crops: 0.5; Irrigated trees: 0.3		
SCROP (DOY_ini -DOY_end)	Irrigated row crops: (60 - 273) Irrigated trees: (196 – 319)		
MAD	Row crops: 0.53 Trees: 1	Row crops: 0.53 Trees: 1	Row crops: 0.53 Trees: 1.395
IrrEff	0.65	0.80	0.90
kx	0.8		
Remarks	No irrigation deficit in Citrus. Low global irrigation efficiency (mainly flood irrigation)	No deficit irrigation applied in trees crops Moderate global irrigation efficiency (higher presence of drip irrigation)	Deficit irrigation applied in trees crops Moderate global irrigation efficiency (higher presence of drip irrigation)

3 Results and discussion

3.1 Sensitivity analysis

3.1.1 Root depth and LAI_{max}

Root depth determines the ability of the soil to store and deliver water, so it is expected that it plays a critical role in controlling the soil moisture dynamics in the atmosphere-plant-soil continuum. Figure 11 shows the impact of changing root depth for all water balance components. sensitivity of the model for the root depth zone. The highest impact is on the generation of surface runoff, with the steepest slope in the sensitivity curve. Setting the scalar in 0.5 - which would mean to reduce by half the soil storage capacity if the remaining soil parameters remain- would result in an increase of 2 times the surface runoff.

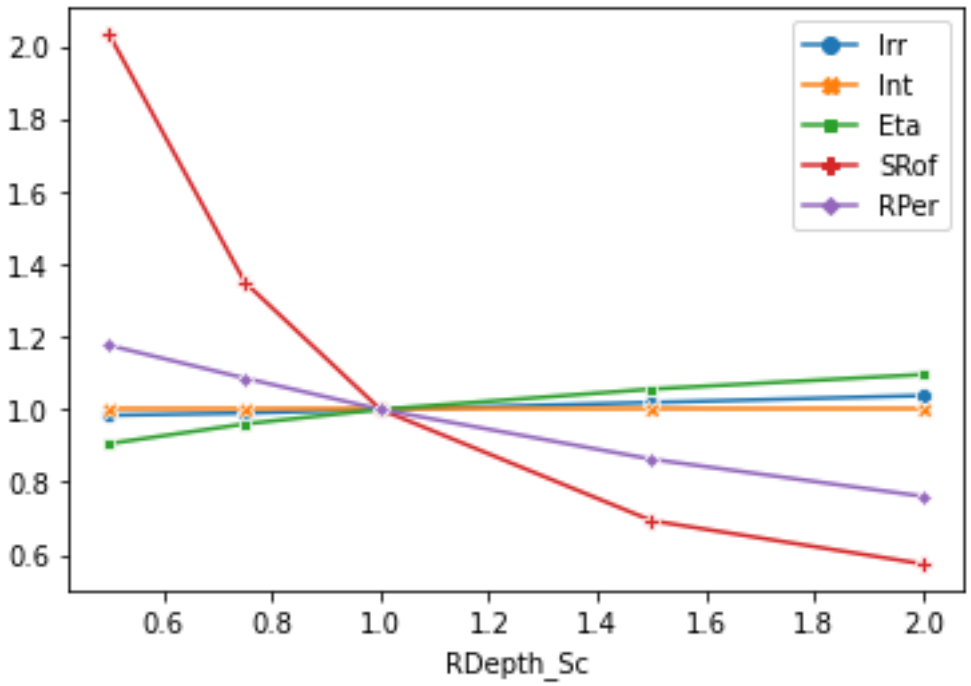

Figure 11. Impact of the Root depth on water balance components.

In SPHY changes in the maximum Leaf Area Index that can reach a “healthy” vegetation with the highest greenness and FPAR, impact the water balance in two ways: 1) direct effect on the canopy interception, and 2) indirectly, as consequence of previous, by controlling the total of water that can be converted into surface runoff or as rainfall infiltration to the root zone

(effective precipitation). Despite this fact, this parameter seems to have a very limited impact on the water balance of the system (Figure 12). As it is shown, the sensitivity of the model to changes in this parameter is almost negligible; the highest impact is observed for the interception component which is reduced by 4% when the LAI_{max} value is scaled by 0.4.

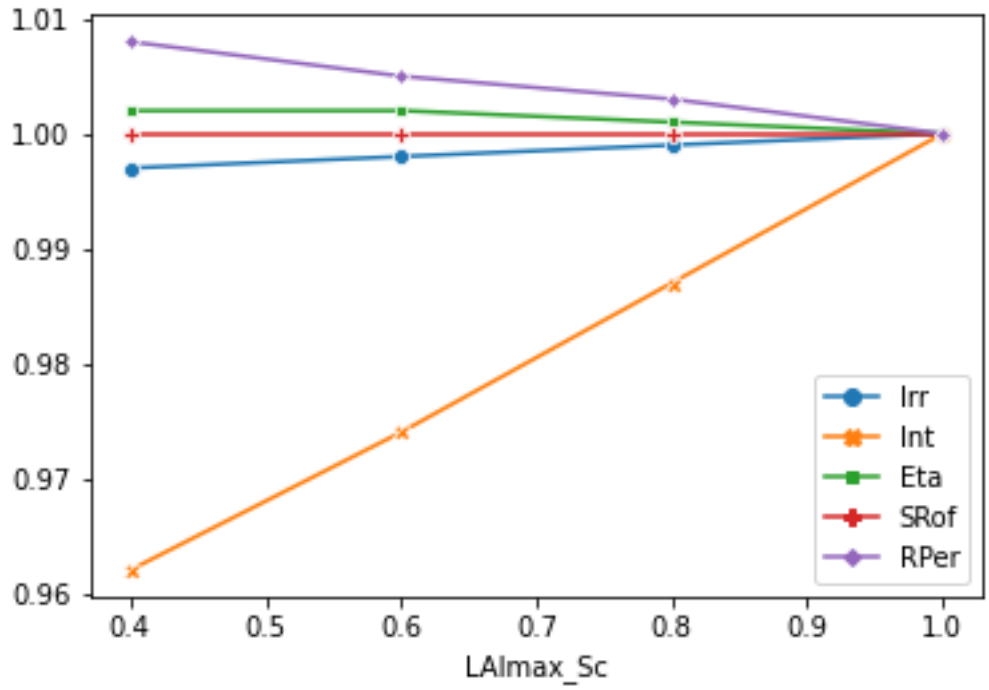

Figure 12. Impact of the LAImax parameter on water balance components.

3.1.2 Irrigation management parameters: Irrigation efficiency and MAD factor

Irrigation efficiency (IrrEff) plays a major role when groundwater recharge is estimated in SPHY-CC. Irrigation is estimated in SPHY-CC as the amount of water that need to be added to the root-zone bucket to fulfill the crop actual evapotranspiration estimated using satellite data. The total irrigation which is applied also includes those potential losses that drain to deeper layers due to the irrigation efficiency of the system. This term, that can be assumed as an irrigation return flow, is directly bypassed to deeper soil layers and computationally added to the percolation that results from the bottom of the root zone (term described in Table 1 as rainfall recharge).

Figure 13 shows the impact of irrigation efficiency parameter in the total (gross) irrigation applied in the system, and the total root percolation. A baseline value of 0.9 has been adopted

for the sensitivity analysis. When IrrEff is reduced from 0.9 to 0.8 (~11%), root percolation is increased by 30%. If efficiency is increased up to 0.95 (%6), the root percolation is reduced by 13%.

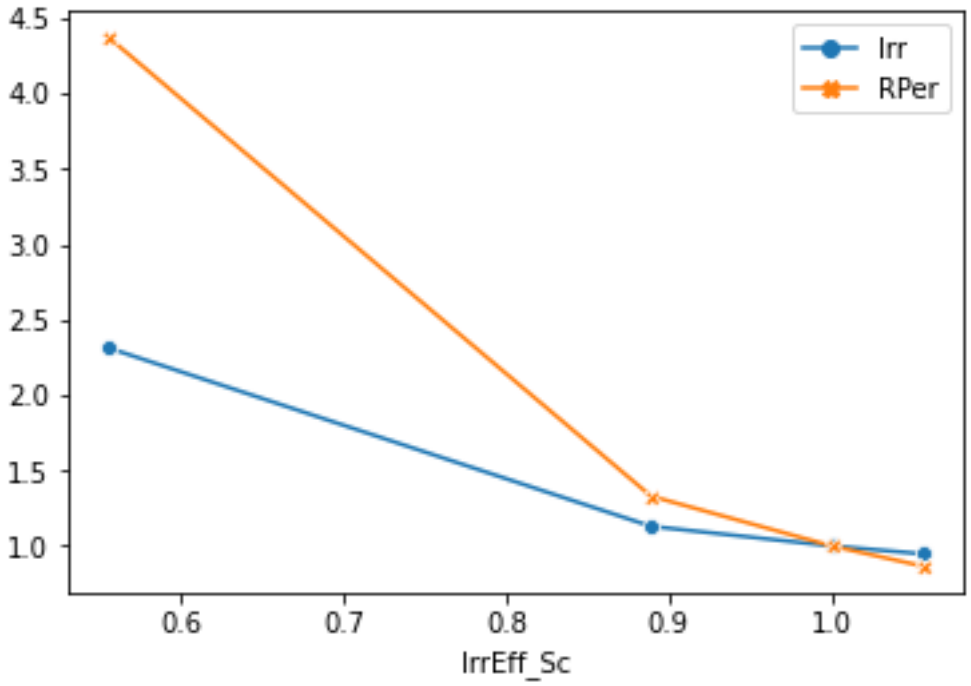

Figure 13. Impact of Irrigation Efficiency on water balance components.

The last parameter evaluated refers to the MAD factor. This parameter modifies the Readily Available Water (RAW) in the root zone by a scalar which simulates the crop tolerance to water stress. Values higher than 1 would suggest high tolerances to plant water stress and hence irrigation inputs may be postponed in time (deficit irrigation). Values lower than 1 are usually used for crops that would require water even when crop stress due to soil moisture shortage is reached. MAD values higher than 1.0 can be linked to irrigation deficit, a practice that started to be implemented in Citrus trees in the Campo de Cartagena catchment in recent years. In the opposite, horticulture crops are extremely sensitive to water stress conditions being a common practice in the region to irrigate them before the onset of soil moisture stress. This practice would be equivalent to set MAD values below 1.0.

To test the impact of different MAD values on the final outputs, baseline figures have been manually modified for “irrigated trees” (landcover #1) and “irrigated row-crops” (landcover #2). Several combinations have been tested and results are shown in Figure 14. As it is shown,

the impact of MAD values in the final outputs seems to be almost negligible for all the configurations simulated.

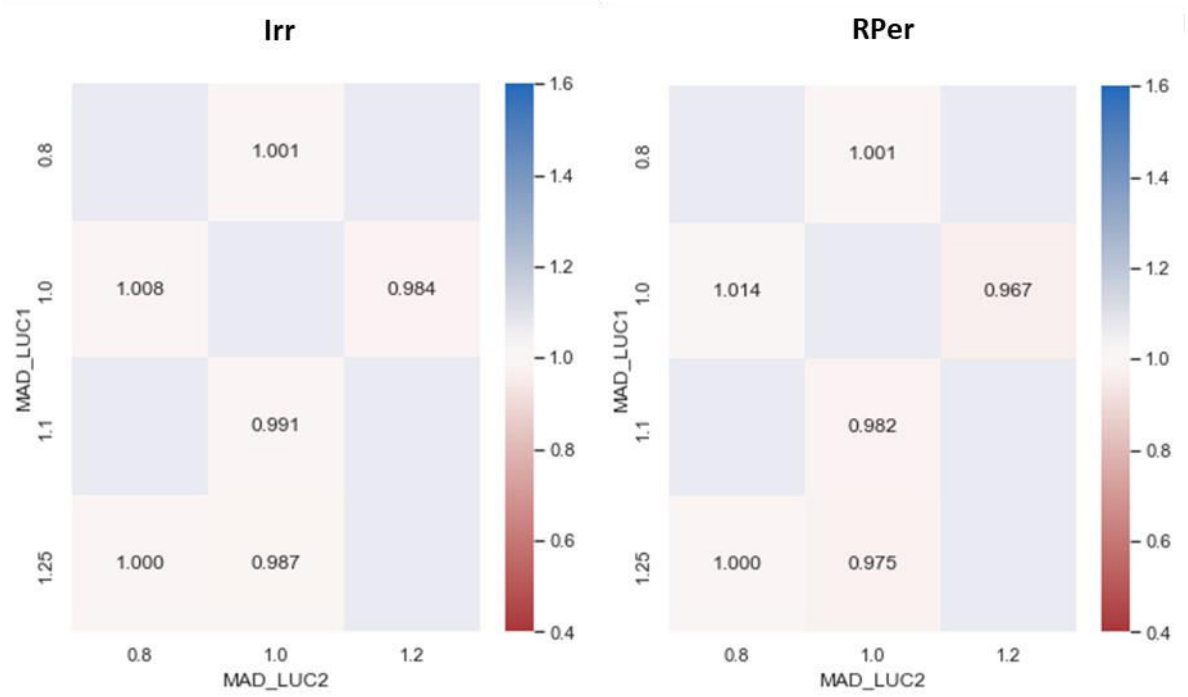

Figure 14. Impact of MAD factor in Irrigation (left) and Root Percolation (right). All values refer to relative deviation against baseline value.

3.1.3 Surface runoff routing (Kx)

As explained in section 2.2.7, surface runoff flows downstream according to the frictions and resistances that act along the drainage or channel network. These resistances are simulated in SPHY through the Kx coefficient. The sensitivity of the SPHY-CC model to Kx was evaluated by comparison of the streamflow curves for different events in the period of study (Figure 15) assuming a RDepth baseline value (RDepth_Sc=1), and others. This combined-sensitivity analysis aims to get the kx-RDepth pair value that best match streamflow observations. Results are shown in Figure 16 and Figure 17. The combination of baseline conditions (kx=0.6, RDepths of 0.3m for row crops, and 0.7m for tress) overestimates streamflows. A reasonable pair-value may be reached at kx = 0.8, RDepth_Sc = 1.2. These values were finally adopted as the “calibrated” values for both parameters.

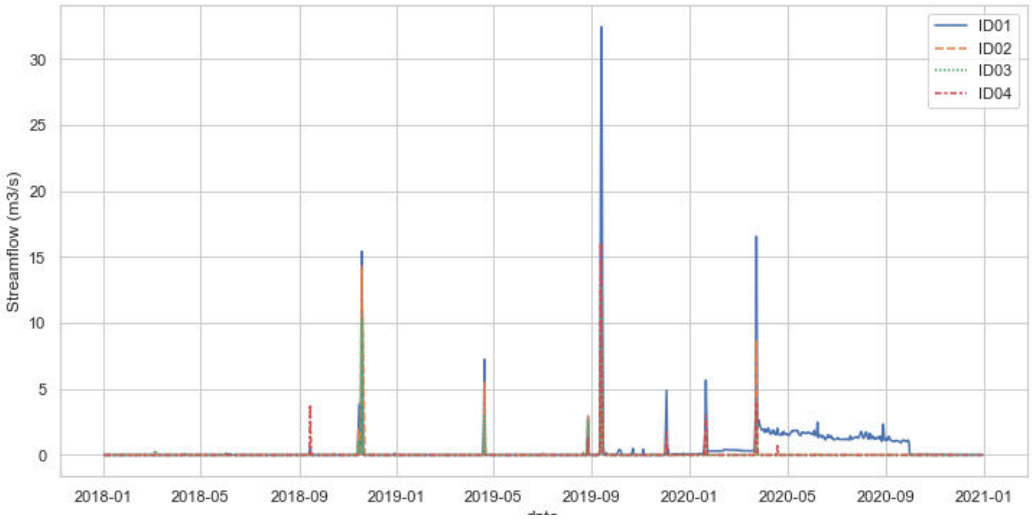

Figure 15. Daily hydrographs of observed streamflows at different gauges.

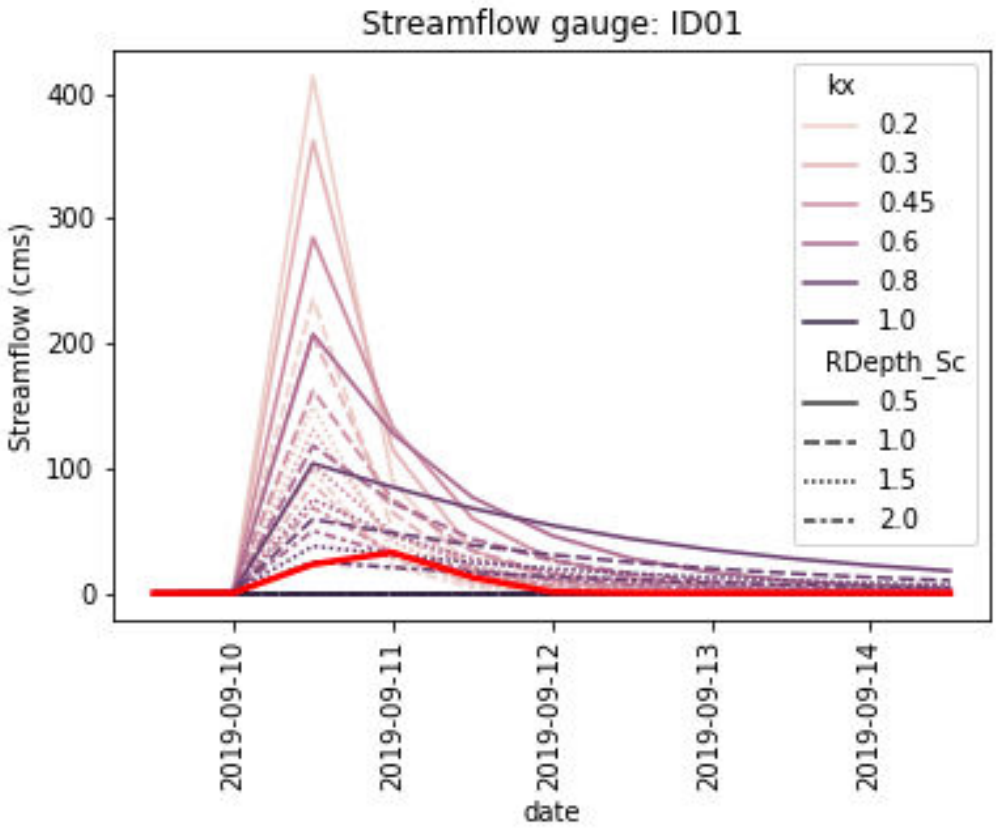

Figure 16. Streamflow curves for the 2019-09 event. SPHY predicted values (purple hues and line styles) vs measurements (thick red line).

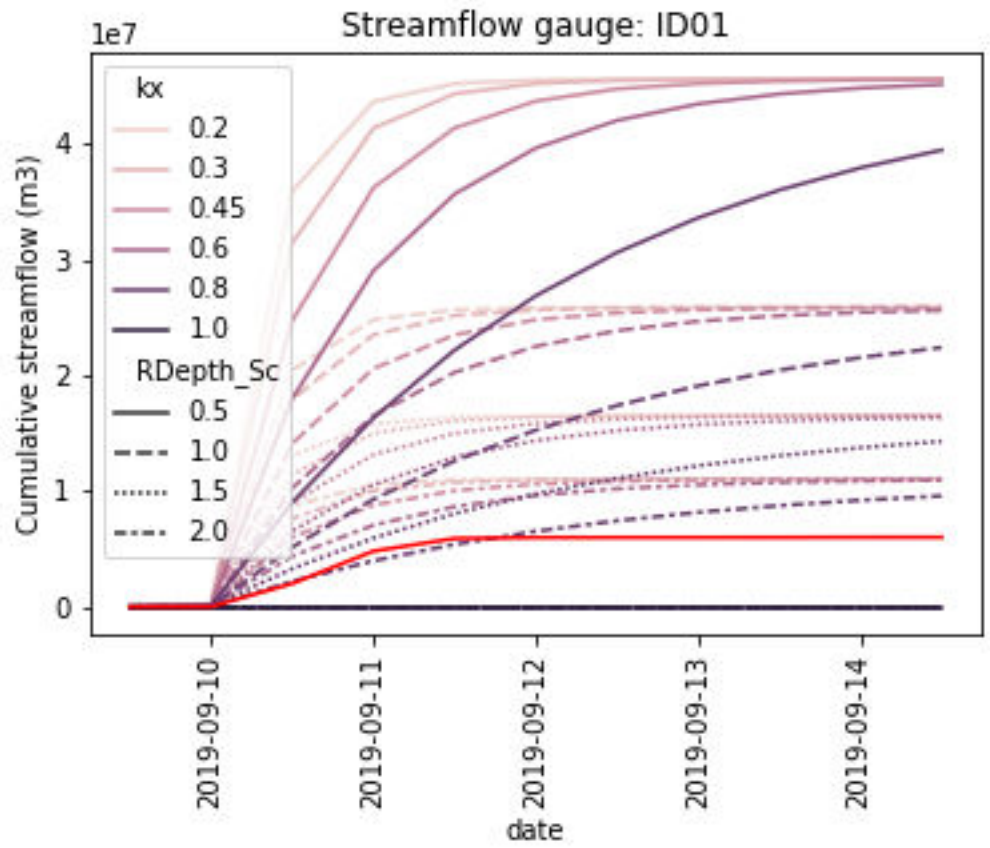

Figure 17. Cumulative streamflow (m^3) during the Sep-2019 rainfall event.

3.2 Verification of outputs

3.2.1 Comparison with irrigation quotas

Yearly values of irrigation water applied at for the area were in close agreement with the "surface" irrigation quotas already delivered by the CRCC (Figure 18). This closure happens with models for which irrigation efficiencies were around 0.90 y 0.95. This agreement is expected to be reached in those years in which the relative contribution of groundwater resources to the total is very limited. Because the CRCC's irrigation data only refers to surface waters, the departure from the model predictions and the real data may be taken as a first approach to the groundwaters pumped from the aquifers.

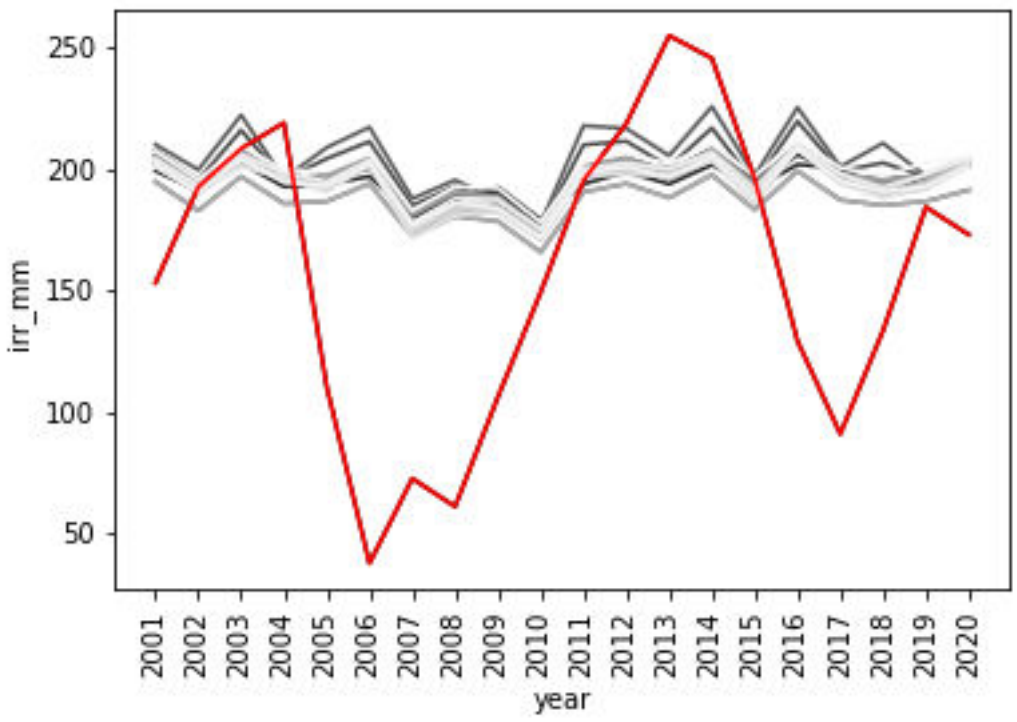

Figure 18. Irrigation water delivered by CRCC (red line) vs SPHY-CC predicted values for different configuration models with irrigation efficiencies of 0.90 and 0.95.

3.3 Current water balance (2000–2020)

Annual figures for the main water balance components in the 2000-2020 period are shown in Figure 19 (interannual variability) and Figure 20 (spatial patterns). In average the total root percolation accounts around 80 mm/year (61 hm^3/year for the recharge area under analysis), which represent around 27% of the mean annual precipitation. Irrigation accounts 127 mm/year, while surface runoff is 12 mm/year (around 10 hm^3/year).

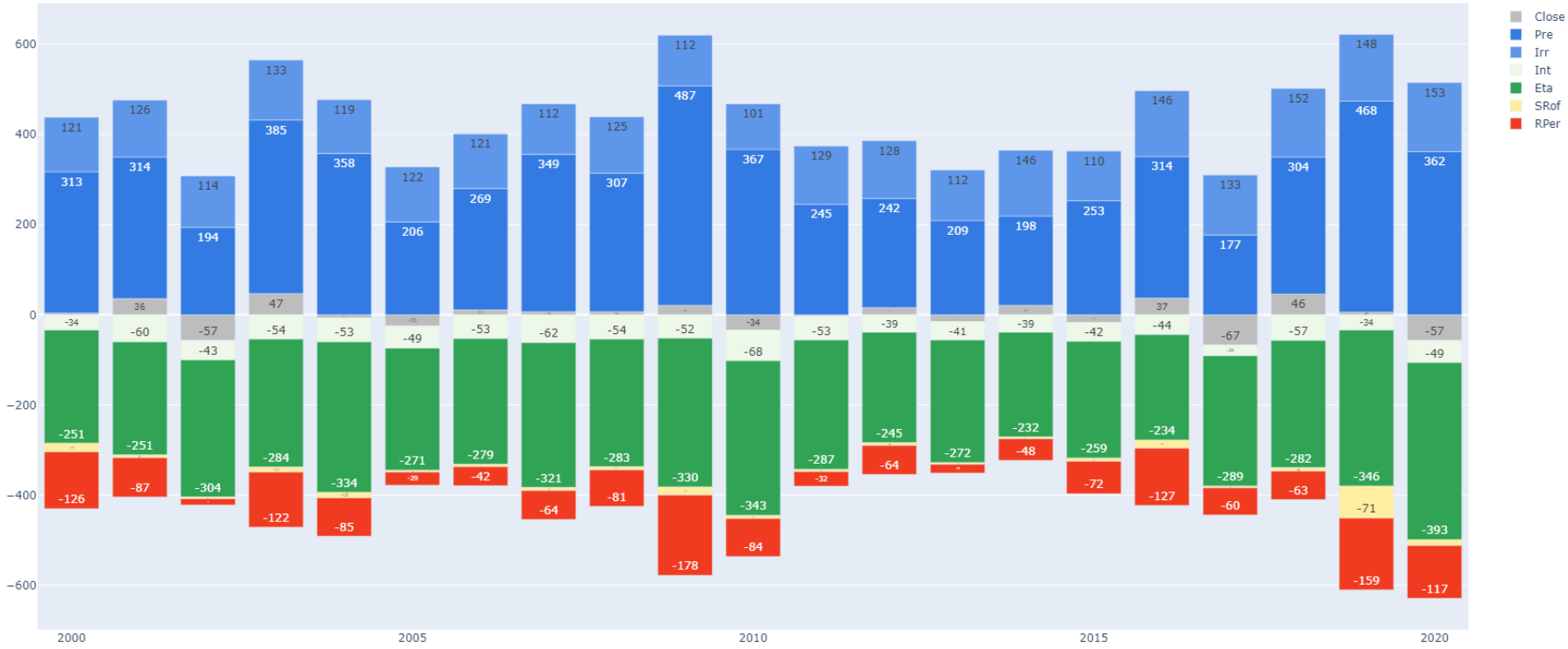

Figure 19. Annual figures of water balance components in the Campo de Cartagena catchment in the 2000-2020 period.

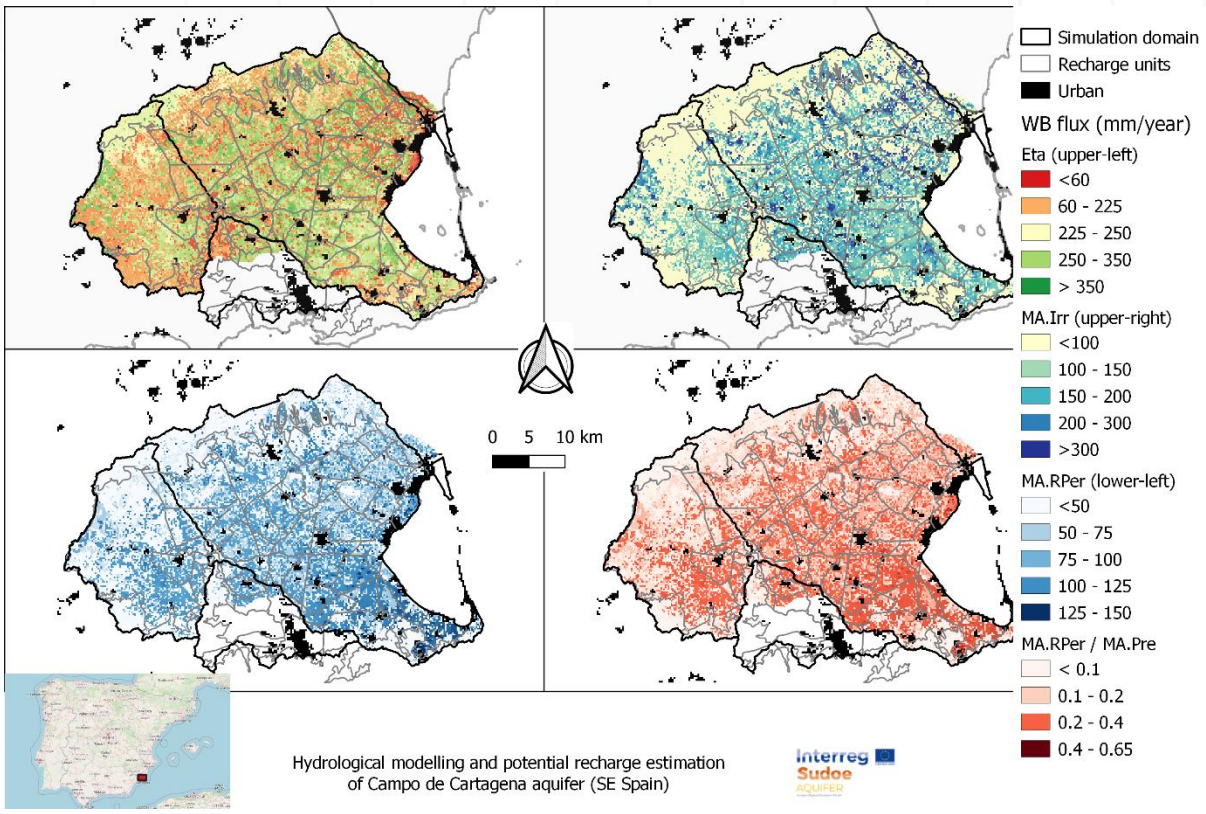

Figure 20. Mean Annual values of the main water balance components in Campo de Cartagena (2000-2020). RPer_ratio refers to the fraction between Root Percolation (MA.RPer) and Precipitation (MA.Pre)

3.4 Historical water balance (1951-1999)

Once calibrated for the 2000-2020 period, the SPHY-CC mode was used to quantify the past patterns of recharge assuming several forcing conditions (see Table 10).

During the 1951-1979 period, the groundwater recharge was influenced mostly by the rainfall patterns, and a very limited level of agricultural development characterized by a strong reliance on groundwater resources pumped from the Quaternary aquifer, and irrigation schemes of very low efficiency. The groundwater recharge in this period has been estimated in 83 mm/year in average, or 63 hm^3/year if this figure is translated for the recharge area of the Quaternary aquifer. The relative contribution of irrigation return flow to the total groundwater recharge was estimated in 16%.

In the 1980-1999 period, groundwater recharge was explained by a strong expansion of the irrigated area driven most likely by the onset of water resources from the Tajo-Segura interbasin aqueduct and better access to groundwater resources. In parallel, irrigation

efficiency increased abruptly due to the fast implementation of drip irrigation techniques (. The convergence of these drivers resulted in a net increase of the total irrigation applied in the system by 50% (from 68 mm/year up to 105 mm). As consequence, groundwater recharge increased by 11% (from 83 to 92 mm/year, or from 52 to 79 hm^3/year for the area of recharge), while the relative contribution of the irrigation return flow to the total groundwater recharge was estimated at 23%.

During the 2000-2020 period, groundwater recharge was driven by an increase of irrigation efficiency and the inclusion of irrigation deficit techniques applied in tree crops. The irrigated area increased moderately mostly due to the conversion of rainfed tree crops into irrigated ones. In average terms, groundwater recharge was estimated in 80 mm/year (60 hm^3/year for the recharge area analysed), a value very similar to the ones simulated for the 1951-1979 period. At this period, the relative contribution of irritation return flow to the total groundwater recharge increased up to 29%.

When interannual values are considered, no significant differences in the generation of recharge have been stated for the sub-periods considered (Figure 22). Still, annual rainfall can be considered as the best predictor of annual groundwater recharge in the region (Figure 23).

Tables 11 and 12 collect mean annual values of main water balance components for different subperiods of analysis and the statistical metrics for the main SPHY-CC water balance components for the period 1951-2020 respectively.

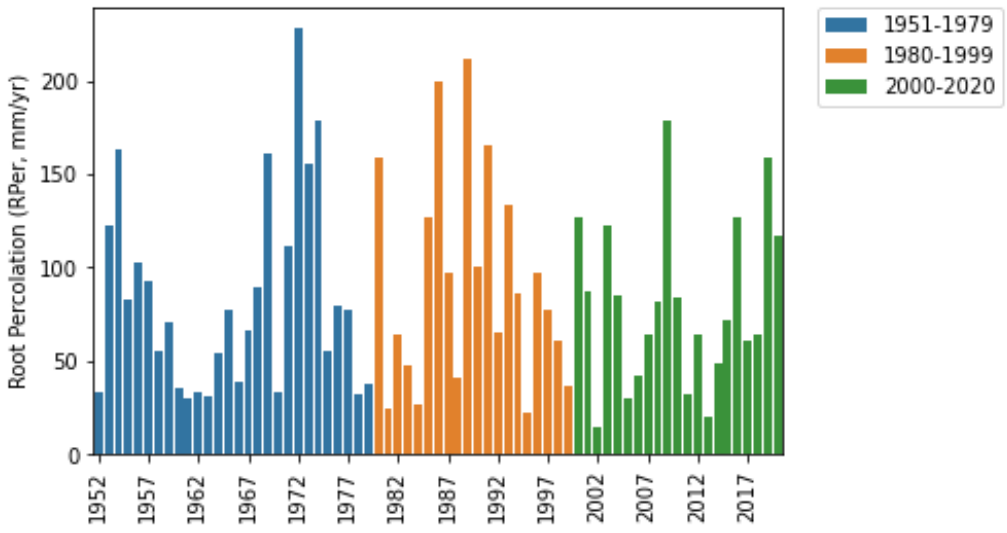

Figure 21. Evolution of root percolation along the period of analysis. Values are grouped according to the sub-period analyzed.

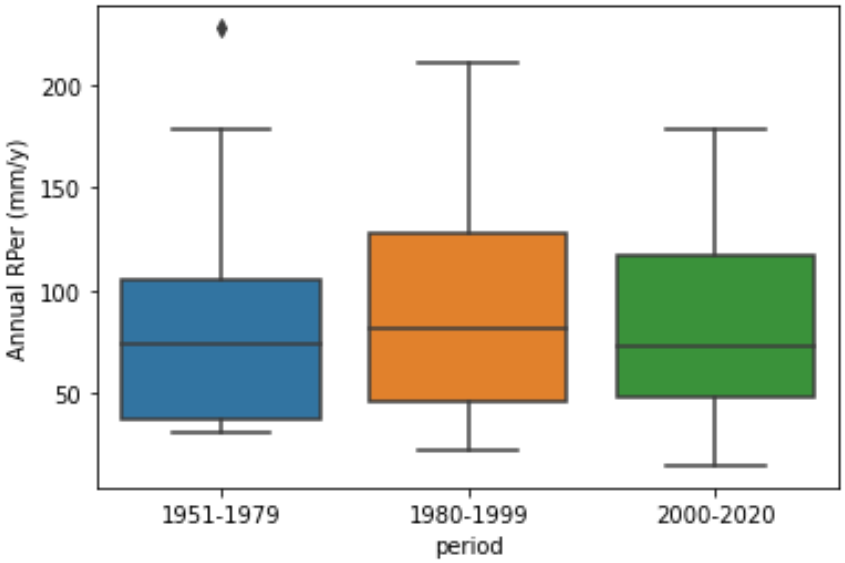

Figure 22. Boxplots with total drainage and annual variability for the three sub-periods analyzed.

Table 11. Mean annual values of main water balance components in Campo de Cartagena for different subperiods of analysis.

	Water depth (mm/y)			Volume* (hm^3/y)		
WB	1951-1979	1980-1999	2000-2020	1951-1979	1980-1999	2000-2020
Pre	299	288	301	227	218	228
Irr	68	105	127	52	79	96
Int	54	47	48	41	36	36
Eta	228	247	290	173	187	220
SRof	3	6	11	2	5	9
RPer	83	92	80	63	70	60
RPer/Pre	0.28	0.32	0.27			

* Water depth and volume figures refer to an area, which excludes Fuente-Álamo subcatchment (see Figure 5).

Table 12. Statistical metrics for the main SPHY-CC water balance components for the period 1951-2020.

	Water depth (mm/y)				Volume* (hm^3/y)			
	Mean	median	min	max	mean	median	min	max
Pre	296	304	95	561	225	231	72	426
Irr	97	91	56	168	73	69	43	128
Int	50	49	24	92	38	37	18	70
Eta	252	252	125	393	191	192	95	298
SRof	6	4	0	71	5	3	0	54
RPer	84	77	14	228	64	58	10	173

* Water depth and volume figures refer to an area, which excludes Fuente-Álamo subcatchment (see Figure 5).

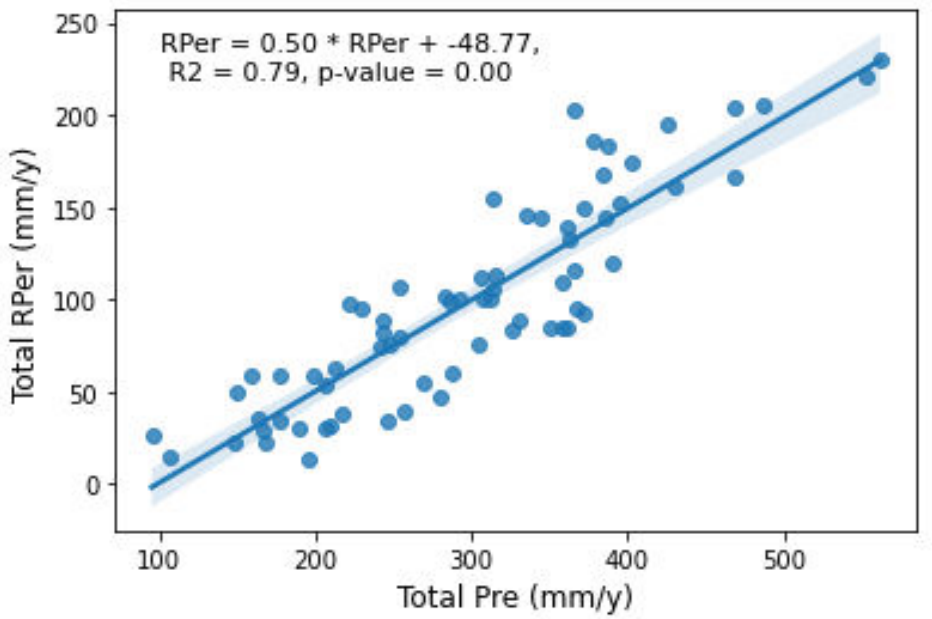

Figure 23. Relationship between annual precipitation and annual drainage for the period of analysis (1951-2020).

4 Conclusions

This study aims to adapt the SPHY model to the Campo de Cartagena catchment (SE Spain) to simulate the water balance in the soil root zone from the 1950s until the end 2020. The new SPHY model adapted to the Campo de Cartagena includes a novel module able to compute irrigation inputs at the pixel level based on satellite data. Due to the particular landscape properties of the region, the root percolation component computed by SPHY is here assumed

as a good proxy of the potential groundwater recharge to the Quaternary aquifer. Timeseries of monthly root percolation spatially aggregated for recharge subunits were computed and used as the main forcing input of the hydrogeological model of the Quaternary aquifer. A sensitivity analysis and calibration process based on intercomparison of SPHY outputs with independent sources of data has been performed to support the simulation exercise.

The combination of climate, land-use change and irrigation-crop management drivers has a primary role on temporal and spatial patterns of groundwater recharge in the region. Our simulation assumptions based on historical developments and local-expert knowledge would suggest no significant differences in the long-term groundwater recharge rates observed during the simulated period (1951-2020). Annual recharge rate has been stated 84 mm/year, with the lowest value reached in the 2000-2020 subperiod (80 mm/year), and the highest one in the 1980-1999 (92 mm/year). The lack of significant differences in average annual recharge rates are explained by the strong interannual variability observed in rainfall patterns, but also by the trade-offs resulting from the combination of climate, land use and irrigation-crop management drivers. Regarding this, the expected rise in groundwater recharge in the aquifer due to increase of the irrigated area, mostly promoted by the onset of “new resources” from the Tajo-Segura interbasin aqueduct at the beginning of the 1980s, may have been strongly compensated by improvements in the irrigation and crop management practices adopted in the area. Our results suggest that the relative contribution of return flows from irrigation to the total recharge has been increased from the beginnings of the 1950s (16%) until recent dates (29%).

5 References

Addor, N., & Melsen, L. A. (2019). Legacy, Rather Than Adequacy, Drives the Selection of Hydrological Models. *Water Resources Research*, *55*(1), 378–390. https://doi.org/10.1029/2018WR022958

Alcolea, A., Contreras, S., Hunink, J. E., García-Aróstegui, J. L., & Jiménez-Martínez, J. (2019). Hydrogeological modelling for the watershed management of the Mar Menor coastal lagoon (Spain). *Science of the Total Environment*, *663*. https://doi.org/10.1016/j.scitotenv.2019.01.375

Allen, R. G., Pereira, L. S., Raes, D., & Smith, M. (1998). *Crop evapotranspiration: Guidelines for computing crop water requirements* (Issue 56). http://www.fao.org/docrep/x0490e/x0490e00.HTM

Beven, K. (1982). On subsurface stormflow: Predictions with simple kinematic theory for saturated and unsaturated flows. *Water Resources Research*, *18*(6), 1627–1633. https://doi.org/10.1029/WR018I006P01627

Beven, K. J. (2012). Rainfall-runoff modelling: the primer. In *Rainfall-Runoff Modelling: The Primer: Second Edition*. John Wiley & Sons, Ltd. https://doi.org/10.1002/9781119951001

Beven, K., & Young, P. (2013). A guide to good practice in modeling semantics for authors and referees. *Water Resources Research*, *49*(8), 5092–5098. https://doi.org/10.1002/WRCR.20393

Bouwer, H. (1969). Infiltration of Water into Nonuniform Soil. *Journal of the Irrigation and Drainage Division*, *95*(4), 451–462.

Cabello, V., & Brugnach, M. (2023). Whose waters, whose nutrients? Knowledge, uncertainty, and controversy over eutrophication in the Mar Menor. *Ambio*, *52*, 1112–1124. https://doi.org/10.1007/s13280

Contreras, S., Alcolea, A., Jiménez-Martínez, J., & Hunink, J. E. (2017). *Cuantificación de la descarga subterránea al Mar Menor mediante modelización hidrogeológica del acuífero superficial Cuaternario*.

Contreras, S., Hunink, J. E., & Baille, A. (2014). *Building a Watershed Information System for the Campo de Cartagena basin (Spain) integrating hydrological modeling and remote*

sensing. http://www.futurewater.nl/wp-content/uploads/2014/07/SIRRIMED_WP5-FutureWater-Report125.pdf

Dam, J. C. van, Huygen, J., Wesseling, J. G., Feddes, R. A., Kabat, P., Walsum, P. E. V. van, Groenendijk, P., & Diepen, C. A. van. (1997). *Theory of SWAP version 2.0; simulation of water flow, solute transport and plant growth in the soil-water-atmosphere-plant environment*. https://www.wur.nl/en/Publication-details.htm?publicationId=publication-way-333036363431

Domingo-Pinillos, J. C., Senent-Aparicio, J., García-Aróstegui, J. L., & Baudron, P. (2018). Long Term Hydrodynamic Effects in a Semi-Arid Mediterranean Multilayer Aquifer: Campo de Cartagena in South-Eastern Spain. *Water 2018, Vol. 10, Page 1320*, *10*(10), 1320. https://doi.org/10.3390/W10101320

Eekhout, J. P. C., Terink, W., & De Vente, J. (2018). Assessing the large-scale impacts of environmental change using a coupled hydrology and soil erosion model. *Earth Surface Dynamics*, *6*(3), 687–703. https://doi.org/10.5194/ESURF-6-687-2018

Faz Cano, A. (2003). El suelo de la Región de Murcia y su potencial Agrícola. In M. Esteve Selma, M. Llorens, & C. Martínez Gallur (Eds.), *Los recursos naturales de la Región de Murcia: Un análisis interdisciplinar* (pp. 161–170). Servicio de Publicaciones, Universidad de Murcia.

Fontaine, T. A., Cruickshank, T. S., Arnold, J. G., & Hotchkiss, R. H. (2002). Development of a snowfall-snowmelt routine for mountainous terrain for the soil water assessment tool (SWAT). *Journal of Hydrology*, *262*(1–4), 209–223. https://doi.org/10.1016/S0022-1694(02)00029-X

Francés, F., Vélez, J. I., & Vélez, J. J. (2007). Split-parameter structure for the automatic calibration of distributed hydrological models. *Journal of Hydrology*, *332*(1–2), 226–240. https://doi.org/10.1016/J.JHYDROL.2006.06.032

Gassman, P. W., Reyes, M. R., Green, C. H., & Arnold, J. G. (2007). The Soil and Water Assessment Tool: Historical Development, Applications, and Future Research Directions. *Transactions of the ASABE*, *50*(4), 1211–1250. https://doi.org/10.13031/2013.23637

Guaita-García, N., Martínez-Fernández, J., Barrera-Causil, C. J., & Fitz, H. C. (2022). Stakeholder analysis and prioritization of management measures for a sustainable development in the social-ecological system of the Mar Menor (SE, Spain). *Environmental Development*, *42*, 100701.

https://doi.org/10.1016/J.ENVDEV.2022.100701

Heber Green, W., & Ampt, G. A. (1911). Studies on Soil Phyics. *The Journal of Agricultural Science*, *4*, 1–24. https://doi.org/10.1017/S0021859600001441

Horton, P., Schaefli, B., & Kauzlaric, M. (2022). Why do we have so many different hydrological models? A review based on the case of Switzerland. *Wiley Interdisciplinary Reviews: Water*, *9*(1), e1574. https://doi.org/10.1002/WAT2.1574

IGME. (1991). *Estudio hidrogeológico del Campo de Cartagena (2a fase)*.

Immerzeel, W. W., van Beek, L. P. H., Konz, M., Shrestha, A. B., & Bierkens, M. F. P. (2012). Hydrological response to climate change in a glacierized catchment in the Himalayas. *Climatic Change*, *110*(3–4), 721–736. https://doi.org/10.1007/S10584-011-0143-4/FIGURES/10

Jiménez-Martínez, J., García-Aróstegui, J. L., Hunink, J. E., Contreras, S., Baudron, P., & Candela, L. (2016). The role of groundwater in highly human-modified hydrosystems: a review of impacts and mitigation options in the Campo de Cartagena-Mar Menor coastal plain (SE Spain). *Environmental Reviews*, *24*(4), 377–392. https://doi.org/10.1139/er-2015-0089

Karssenberg, D., Burrough, P. A., Sluiter, R., & de Jong, K. (2001). PCRaster software and course materials for teaching numerical modelling in the environmental sciences. *Transactions in GIS*, *5*(2), 99–110. https://doi.org/10.1111/1467-9671.00070

Liang, X., Wood, E. F., & Lettenmaier, D. P. (1996). Surface soil moisture parameterization of the VIC-2L model: Evaluation and modification. *Global and Planetary Change*, *13*(1–4), 195–206. https://doi.org/10.1016/0921-8181(95)00046-1

MITECO. (2019). *Análisis de soluciones para el objetivo del vertido cero al Mar Menor proveniente del Campo de Cartagena.*

Morgan, R. P. C., & Duzant, J. H. (2008). Modified MMF (Morgan–Morgan–Finney) model for evaluating effects of crops and vegetation cover on soil erosion. *Earth Surface Processes and Landforms*, *33*(1), 90–106. https://doi.org/10.1002/ESP.1530

O'Green, A. T. (2013). Soil Water Dynamics. *Nature Education Knowledge*, *4*(5), 9. https://www.nature.com/scitable/knowledge/library/soil-water-dynamics-103089121/#url

Peral García, C., Fernández-Victorio, N., Calzado, B., & Ramos, P. (2017). *Serie de precipitación diaria en rejilla con fines climáticos*.

https://www.aemet.es/documentos/es/conocermas/recursos_en_linea/publicaciones_y_estudios/publicaciones/NT_24_AEMET/NT_24_AEMET.pdf

Pettorelli, N., Vik, J. O., Mysterud, A., Gaillard, J.-M., Tucker, C. J., & Stenseth, N. C. (2005). Using the satellite-derived NDVI to assess ecological responses to environmental change. *Trends in Ecology & Evolution*, *20*(9), 503–510. https://doi.org/10.1016/j.tree.2005.05.011

Pôças, I., Calera, A., Campos, I., & Cunha, M. (2020). Remote sensing for estimating and mapping single and basal crop coefficientes: A review on spectral vegetation indices approaches. *Agricultural Water Management*, *233*, 106081. https://doi.org/10.1016/J.AGWAT.2020.106081

Pôças, I., Paço, T., Paredes, P., Cunha, M., & Pereira, L. (2015). Estimation of actual crop coefficients using remotely sensed vegetation indices and soil water balance modelled data. *Remote Sensing*, *7*(3), 2373–2400. https://doi.org/10.3390/rs70302373

Puertes, C., Bautista, I., Lidón, A., & Francés, F. (2021). Best management practices scenario analysis to reduce agricultural nitrogen loads and sediment yield to the semiarid Mar Menor coastal lagoon (Spain). *Agricultural Systems*, *188*. https://doi.org/10.1016/j.agsy.2020.103029

Samper, J., Pisani, B., Alvares, D., & García, M. A. (2007). GIS-BALAN: Un modelo hidrológico semi-distribuido acoplado a un Sistema de Información Geográfica para la estimación de los recursos hídricos. In J. V. Giráldez Cervera & F. J. Jimeneze Hornero (Eds.), *Estudios de la Zona No Saturada del Suelo Vol. VIII* (pp. 341–346).

Sandonnini, J., Del Pilar Ruso, Y., Cortés Melendreras, E., Barberá, C., Hendriks, I. E., Kersting, D. K., & Giménez Casalduero, F. (2021). The emergent fouling population after severe eutrophication in the Mar Menor coastal lagoon. *Regional Studies in Marine Science*, *44*, 101720. https://doi.org/10.1016/J.RSMA.2021.101720

Senent-Aparicio, J., López-Ballesteros, A., Nielsen, A., & Trolle, D. (2021). A holistic approach for determining the hydrology of the Mar Menor coastal lagoon by combining hydrological & hydrodynamic models. *Journal of Hydrology*, *603*. https://doi.org/10.1016/j.jhydrol.2021.127150

Terink, W., Lutz, A. F., Simons, G. W. H., Immerzeel, W. W., & Droogers, P. (2015). SPHY v2.0: Spatial Processes in HYdrology. *Geoscientific Model Development*, *8*(7), 2009–2034. https://doi.org/10.5194/gmd-8-2009-2015

Van Beek, L. P. H., Wada, Y., & Bierkens, M. F. P. (2011). Global monthly water stress: 1. Water balance and water availability. *Water Resources Research*, *47*(7). https://doi.org/10.1029/2010WR009791